(4)

AD-A202 278

Substorms, Plasmoids, Flux Robes, and Magnetotail Flux Loss on March 25, 1983: CDAW-8

D. H. FAIRFIELD, D. N. BAKER, and J. A. SLAVIN
Laboratory of Extraterrestrial Physics
NASA Goddard Space Flight Center
Greenbelt, MD 20711

J. D. CRAVEN and L. A. FRANK
University of Iowa
Iowa City, IW 52242

R. C. ELPHIC
University of California at Los Angeles
Los Angeles, CA 90024

J. F. FENNELL
Space Sciences Laboratory
The Aerospace Corporation
El Segundo, CA 90245

I. G. RICHARDSON
Imperial College
London, UK

H. J. SINGER
Air Force Geophysics Laboratory
Hanscom AFB, MA 01731

B. T. TSURUTANI
Jet Propulsion Laboratory
Pasadena, CA 91109

and

R. D. ZWICKI
Los Alamos National Laboratory
Los Alamos, NM 87545

3 October 1988

Prepared for

SPACE DIVISION
AIR FORCE SYSTEMS COMMAND
Los Angeles Air Force Base
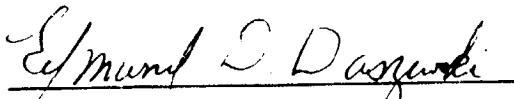P.O. Box 92960
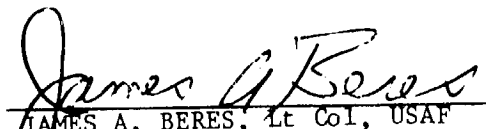Los Angeles, CA 90009-2960

88 1122 048

This report was submitted by The Aerospace Corporation, El Segundo, CA 90245, under Contract No. F04701-85-C-0086 with the Space Division, P.O. Box 92960, Worldway Postal Center, Los Angeles, CA 90009-2960. It was reviewed and approved for The Aerospace Corporation by H. R. Rugge, Director, Space Sciences Laboratory.

Major Edmund D. Daszewski SD/WE was the project officer for the Mission-Oriented Investigation and Experimentation (MOIE) Program.

This report has been reviewed by the Public Affairs Office (PAS) and is releasable to the National Technical Information Service (NTIS). At NTIS, it will be available to the general public, including foreign nationals.

This technical report has been reviewed and is approved for publication. Publication of this report does not constitute Air Force approval of the report's findings or conclusions. It is published only for the exchange and stimulation of ideas.

EDMUND D. DASZEWSKI, Major, USAF
MOIE Project Officer
SD/WE

JAMES A. BERES, Lt Col, USAF
Director, AFSTC West Coast Office

REPORT DOCUMENTATION PAGE

1a. REPORT SECURITY CLASSIFICATION Unclassified	1b. RESTRICTIVE MARKINGS
2a. SECURITY CLASSIFICATION AUTHORITY	3. DISTRIBUTION/AVAILABILITY OF REPORT Approved for public release; distribution unlimited.
2b. DECLASSIFICATION/DOWNGRADING SCHEDULE	
4. PERFORMING ORGANIZATION REPORT NUMBER(S) TR-0088(3940-05)-1	5. MONITORING ORGANIZATION REPORT NUMBER(S) SD-TR-88-85

6a. NAME OF PERFORMING ORGANIZATION The Aerospace Corporation Laboratory Operations	6b. OFFICE SYMBOL (If applicable)	7a. NAME OF MONITORING ORGANIZATION Space Division
6c. ADDRESS (City, State, and ZIP Code) El Segundo, CA 90245		7b. ADDRESS (City, State, and ZIP Code) Los Angeles Air Force Base Los Angeles, CA 90009-2960

8a. NAME OF FUNDING/SPONSORING ORGANIZATION	8b. OFFICE SYMBOL (If applicable)	9. PROCUREMENT INSTRUMENT IDENTIFICATION NUMBER F04701-85-C-0086
8c. ADDRESS (City, State, and ZIP Code)		10. SOURCE OF FUNDING NUMBERS

	PROGRAM ELEMENT NO.	PROJECT NO	TASK NO	WORK UNIT ACCESSION NO.

11. TITLE (Include Security Classification)

Substorms, Plasmoids, Flux Ropes, and Magnetotail Flux Loss on March 25, 1983: CDAW-8

12. PERSONAL AUTHOR(S) Fairfield, D. H., Baker, D. N. and Slavin, J. A. (NASA Goddard Space

13a. TYPE OF REPORT	13b. TIME COVERED FROM _____ TO _____	14. DATE OF REPORT (Year, Month, Day) 1988 October 3	15. PAGE COUNT 70

16. SUPPLEMENTARY NOTATION

17. COSATI CODES			18. SUBJECT TERMS (Continue on reverse if necessary and identify by block number)
FIELD	GROUP	SUB-GROUP	Geosynchronous orbit Magnetospheric variations Solar wind Plasma sheet

19. ABSTRACT (Continue on reverse if necessary and identify by block number)

During a 9-hour period following a storm-sudden commencement on March 25, 1983, six spacecraft near geosynchronous orbit, one over the pole, and three in the magnetotail, monitored a complex sequence of magnetospheric variations. Magnetic field compressions associated with the sudden commencement were seen first by the near earth spacecraft and subsequently by the three down-tail spacecraft with increasing time delays that were consistent with the tailward movement of an interplanetary-shock-associated pressure enhancement. Ground magnetograms and synchronous orbit data are used to identify 7 substorm intensifications during this geomagnetically active period. Six of these intensifications are clearly associated with tail lobe field decreases $\sim 18\ R_E$ behind the earth. Four of these intensifications are followed by both B_z field increases in the tail lobes at ~ 18 and $\sim 30\ R_E$ and by the subsequent observation of rapidly flowing plasma sheet plasma at ISEE 3 $\sim 110\ R_E$ down the tail. During two substorms where DE 1 was optically observing the auroral oval, the area of the polar cap was observed to decrease as the tail lobe field decreased at $18\ R_E$. All these observations are

20. DISTRIBUTION/AVAILABILITY OF ABSTRACT ☐ UNCLASSIFIED/UNLIMITED ☐ SAME AS RPT ☐ DTIC USERS	21. ABSTRACT SECURITY CLASSIFICATION
22a. NAME OF RESPONSIBLE INDIVIDUAL	22b. TELEPHONE (Include Area Code) Unclassified	22c. OFFICE SYMBOL

DD FORM 1473, 84 MAR   83 APR edition may be used until exhausted   SECURITY CLASSIFICATION OF THIS PAGE
All other editions are obsolete.

12. PERSONAL AUTHOR(S) (Continued)

Flight Center); Craven, J. D., Frank, L. A. (University of Iowa); Elphic, R. C. (UCLA), Fennell, J. F. (The Aerospace Corporation); Richardson, I. G. (Imperial College - London UK), Singer, H. J. (Hanscom AFB); Tsurutani, B. T. (JPL); and Zwick, R. D. (Los Alamos National Laboratory)

19. ABSTRACT (Continued)

consistent with the substorm associated release of a plasmoid at a neutral line near 20 R_E; however, the classical north-south variation of the plasma sheet magnetic field, thought to be characteristic of the passage of a plasmoid in the deep tail, was not seen in every case.

PREFACE

A-1

1

CONTENTS

FIGURES

1. INTRODUCTION

Innumerable studies of the complicated interaction of the solar wind with the earth's magnetosphere have led to an evolving and increasingly sophisticated model of energy transfer and dissipation. At times a sudden increase in solar wind pressure, such as that associated with an interplanetary shock, compresses the magnetosphere and produces a storm sudden commencement (ssc) [e.g. Smith et al., 1986]. More generally, transfer of energy to the magnetosphere is regulated by the direction of the interplanetary magnetic field. In the presence of a southward interplanetary field, magnetic flux is transferred from the dayside magnetosphere to the geomagnetic tail [e.g. Baker et al., 1984b]. This flux transfer moves the subsolar magnetopause closer to the earth [Aubry et al., 1970; Fairfield, 1971; Holzer and Slavin, 1978] while causing enhanced flaring of the tail boundary to encompass a larger diameter magnetotail [Maezawa, 1975]. This flaring magnetotail is compressed by a larger component of solar wind pressure producing a stronger tail lobe magnetic field with typically 10^{22} ergs of stored energy. The development of this stressed high-field magnetotail is accompanied by a thinning of the near-earth plasma sheet that separates the tail lobes. The northward field component within the plasma sheet also decreases at this time [e.g. Fairfield, 1984] particularly in the tail region within 20 R_E of the earth [Fairfield, 1986b]. A small B_z component in the inner magnetotail may make the tail more susceptible to magnetic reconnection via the tearing mode instability [e.g. Schindler and Birn, 1982] and the formation of a near-earth neutral line. The energy released by magnetic reconnection at such a neutral line is thought by many workers to cause the onset of the expansive phase of a magnetospheric substorm [e. g. Baker et al., 1984b].

On the earthward side of such a near-earth neutral line, the reconnection model predicts the earthward movement of energetic plasma and the dipolarization of the field in the inner magnetotail. Cross-tail currents are diverted down field lines in the postmidnight magnetosphere where they flow westward through the auroral ionosphere creating the auroral electrojet. The currents then return to the magnetosphere in the premidnight sector. The integrated effect of this diverted current produces magnetic field perturbations at midlatitude ground magnetic observatories and at the geosynchronous orbit, all of which are valuable diagnostics in determining times and longitudes of substorm onset [Clauer and McPherron, 1974; Rostoker et al., 1980, Lester et al., 1983; Singer et al., 1987; Nagai, 1987].

On the tailward side of the neutral line, closed loops of magnetic flux are thought to be created in the plasma sheet which are ejected down the tail once tail lobe fields begin to reconnect at the neutral line [Hones, 1979]. The tailward-flowing plasma containing such flux loops is known as a plasmoid [Hones 1979] and signatures of such structures have been detected in the distant tail by the ISEE 3 spacecraft [e.g. Hones et al., 1984; Baker et al., 1987 and references therein]. This sudden release of stored energy and magnetic flux allows the remaining lobe field lines to expand into the newly available volume thus decreasing both the tail lobe field strength and the diameter of the tail lobe [Maezawa, 1975; Baker et al., 1984a; 1984b]. Since magnetic field lines emanating from the polar cap comprise the magnetic field lines of the magnetotail lobes, the area of the polar cap should decrease as reconnection converts open lobe field lines into closed plasma sheet field lines.

Although the above model is based on observations, and virtually all of the

8

phenomena described above have been observed with varying degrees of clarity, seldom have the majority of these phenomena been observed simultaneously during individual events. The work reported below utilizes the large CDAW-8 data base to illustrate the occurrence of most of these phenomena during a series of substorms that occur on a single day. Section 2 describes the locations of 10 spacecraft used in this study and section 3 briefly reviews the geomagnetic activity. This activity is more fully discussed in Appendix A. Section 4 emphasizes the near-tail ($R<31$ R_E) magnetic field measurements and section 5 discusses the changing area of the polar cap and its relation to magnetotail structure. Section 6 investigates 4 substorm-related observations of the plasma sheet at ISEE 3 in the deep tail and Section 7 summarizes the observations and discusses them in relation to previous work on plasmoids, flux ropes and magnetotail flux loss during substorms.

2. SPACECRAFT LOCATIONS

On March 25 1983 there were three spacecraft in the geomagnetic tail at distances from the earth greater than 15 R_E and seven other spacecraft at and within the 6.6-R_E distance of the geosynchronous orbit. Figure 1a shows various spacecraft trajectories projected in the solar magnetospheric X-Y plane for the time period 0500-1400 UT on this day. The orbit of the DE 1 spacecraft with its apogee of 4.6 R_E over the South Pole is not shown. IMP 8 was located 30.5 R_E from the earth and slightly duskward of the earth-sun line while ISEE 1 was positioned between 17 and 19.5 R_E and slightly dawnward of the earth-sun line. The SCATHA spacecraft was just within the geosynchronous orbit and moved from 1400 LT through dusk to 0200 LT during the period of interest. Five circular arcs outside geosynchronous orbit indicate the local times traversed by five geosynchronous spacecraft between 0500 and 1400 UT. The ISEE-3 spacecraft was 107-110 R_E downstream at this time, off the scale of Figure 1a.

Figure 1b is a solar magnetospheric Y-Z projection which identifies the locations of the three most distant spacecraft. IMP 8 and ISEE 1 were located within the tail lobe between 7 and 12 R_E south of the equatorial plane, while ISEE 3 was about 3.5 R_E north of the equatorial plane. Although ISEE 3 was less than 4 R_E from the earth-sun line, after correcting for a nominal 4° aberration it would be located about 10 R_E dawnward of the center of the tail. This location would normally place ISEE 3 continually within the tail, but measurements shown in Figure 2 indicate otherwise.

Figure 2 displays the thermal electron density measured by the Los Alamos National Laboratory plasma instrument on ISEE 3 (described more fully below) for the time interval 1000-1400 UT. The magnitude and orientation of the
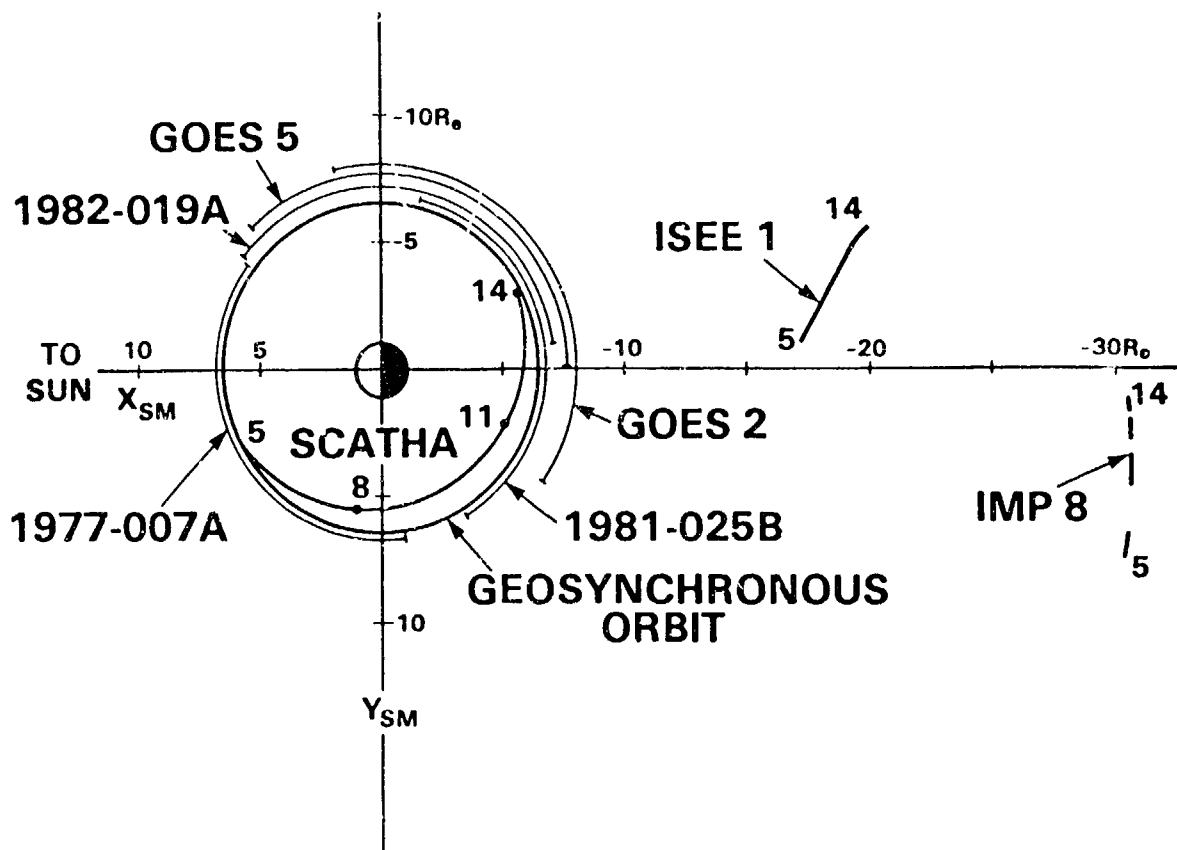
Fig. 1a. Trajectories of various spacecraft projected in the solar
magnetospheric X-Y plane. The arcs surrounding the circle at 6.6 R_E indicate
various spacecraft positions between 5 and 14 hours UT on March 25 1983 .
The ISEE-3 spacecraft is off scale at X=-110 R_E.
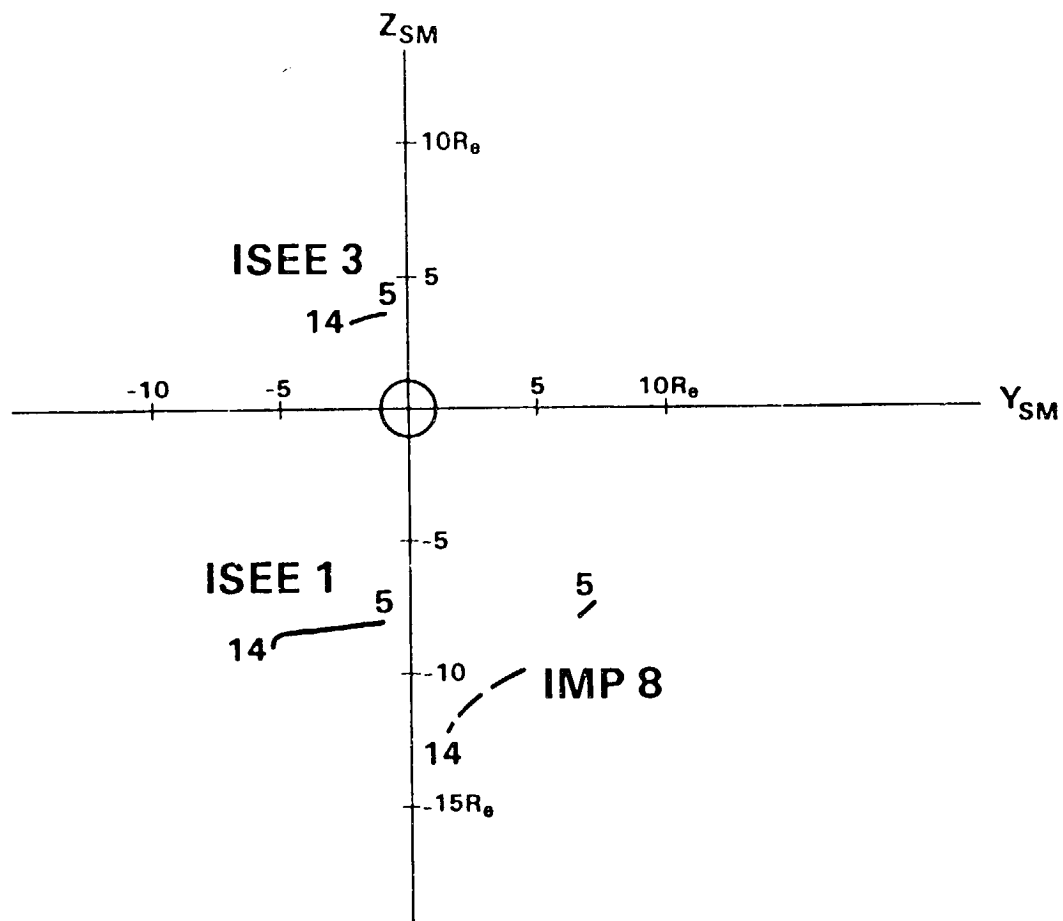
Fig. 1b. Trajectories of three magnetotail spacecraft projected in the solar magnetospheric Y-Z plane.
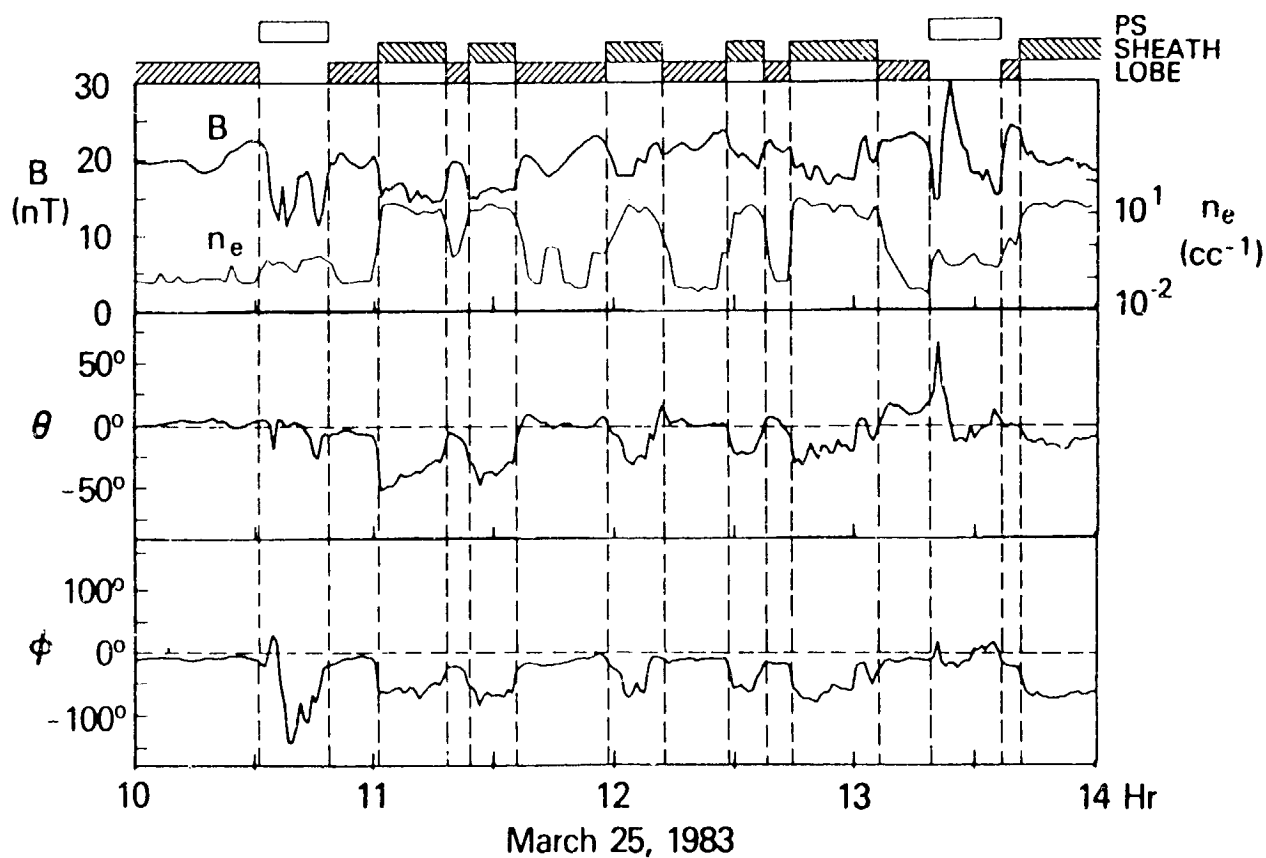
Fig. 2. ISEE 3 data from 1000 to 1400 UT. Vertical lines indicate transitions between the plasma sheet, the tail lobes and the magnetosheath. Tail lobe intervals are characterized by fields aligned near the earth-sun line (θ=0°, ϕ=0°) but the slightly negative values of ϕ indicate skewing of the tail that is necessary to place ISEE 3 near the magnetosheath.

magnetic field are also shown with the latitude and longitude angles in GSM coordinates. The figure contains a number of intervals of high (≥ 1/cc) thermal electron densities when the field is non-taillike and the flow velocities (e.g. see Figures 8 and 9) are near 500 km/s. These observations indicate that the spacecraft was intermittently within the magnetosheath during this interval. Since such observations are not expected if the solar wind is flowing radially from the sun, there are apparently unusual conditions prevailing at this time. If the tail is supposed to be circular with a radius of 25 R_E at the ISEE-3 distance, it would require, in addition to the nominal 4° tail aberration, a 9° departure from the radial solar wind to skew the tail and cause ISEE 3 to enter the magnetosheath. Such an extremely non-radial solar wind direction would be unusual [e.g. Wolfe, 1972] but this hypothesis does receive support from the azimuthal lobe field angles measured by ISEE 3 between magnetosheath intervals (Figure 2), which generally lie between -10° and -20° rather than nearer a nominal value of -4°.

3. GEOMAGNETIC ACTIVITY

March 25 1983 was a disturbed day with an average K_p value of about 5 for the interval of 5-14 hours. Figure 3 contains mid-latitude magnetograms spanning a 10-hour range of local times from the western United States (Boulder, Tucson and Lompoc) through the Pacific (Guam) to the Soviet Union (Irkutsk). (Station locations and abbreviations for these stations and others used in this paper are given in Table 1.) At all these stations a storm sudden commencement is evident at 0544 UT in the B_x, or equivalently the H component. The prompt development of the storm main phase is particularly evident at Guam, the lowest latitude station. The D_{st} index reached a minimum of -90 nT during the 8th hour on this day and recovered to only -86 nT in the 13th hour which is consistent with the B_x depression at Guam during this period. The vertical dashed lines in Figure 3 designate seven substorm intensification or onset times that have been determined from Figure 3, from a number of other magnetograms, and from particle and field data measured by 5 spacecraft at and near synchronous orbit. These determinations and their supporting data are discussed further in Appendix A.
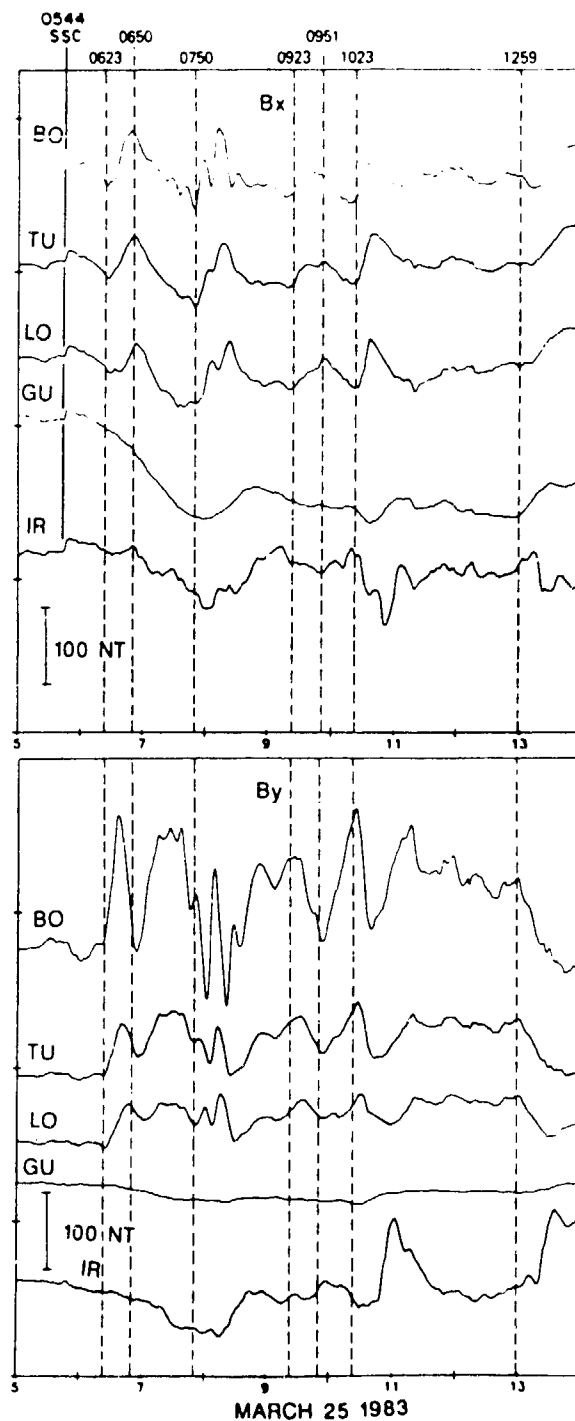
Fig. 3. Horizontal components of midlatitude magnetograms in the geomagnetic north (B_x at top) and east (B_y at bottom) directions. Stations span a 10 hour range of local times from the central United States (BO) to the Soviet Union (IR). Vertical dashed lines indicate the times of substorm intensifications indicated by these stations and other ground and spacecraft measurements as described in the appendix. The solid line through the B_x component indicates the storm sudden commencement at 0544.

18

Table 1. Magnetogram Stations and Locations

Name	Abbreviation	Geomag. Coord. Lat	Long
Figure 2 - midlatitude			
Boulder	BO	49.5	316.5
Tucson	TU	40.4	312.2
Lompoc	LO	41.4	300.8
Guam	GU	4.0	212 9
Irkutsk	IR	40.7	174.8
Figure 10 - AFGL chain plus St Johns			
Newport	NW	55.1	300.0
Rapid City	RC	53.4	317.5
Camp Douglas	CD	54.6	333.1
Mt Clemens	MC	53.9	342.5
Sudbury	SD	53.9	357.1
St Johns	SJ	59.1	18.9
Figure 11 - Auroral zone			
Barrow	BA	68.5	241.1
Yellowknife	YE	69.1	292.6
Meanook	ME	61.8	301.0
Ft Churchill	FC	68.7	322.8
Great Whale River	GW	66.6	347.4
Others not shown			
Leirvogur	LRV	70.2	71.0
College	CMO	64.6	256.5
Kiruna	KIR	65.3	115.6
Sitka	SIT	60.0	275.3
Glenlea	GLL	59.5	320.0
Victoria	VIC	54.2	293.0
Fredricksburg	FRD	49.6	349.8
San Juan	SJG	29.6	3.1
Honolulu	HON	21.1	266.5

4. NEAR-EARTH TAIL MEASUREMENTS

The magnetic field magnitudes measured by SCATHA and the three tail spacecraft are shown in Figure 4. SCATHA near the 1500 LT meridian saw a large, sudden field increase at 0544 UT which undoubtedly was caused by an increase in the total pressure exerted by the solar wind on the magnetosphere. This field magnitude increase is the magnetospheric manifestation of the sudden commencement observed at ground level and is probably due to an interplanetary shock. A similar increase in field magnitude was detected successively by ISEE 1, IMP 8 and ISEE 3 at 0549, 0552 and 0608 UT, as marked on the figure. Using the GSM X positions of the four spacecraft at 4.5, -17.5, -30.5 and -110 R_E, propagation velocities from SCATHA to the three more tailward spacecraft were computed to be 468, 465 and 507 km/s respectively. Although time estimates may be uncertain by as much as 30 s, leading to uncertainties in the velocity as large as 50 km/s, these calculated velocities imply slightly higher solar wind velocities of perhaps 550 km/s that are reduced to the observed average velocities of 470 km/s in the near-earth magnetosheath and increase above 500 km/s in the downstream magnetosheath [e.g. Stahara et al., 1980].

After the significant increase in magnetic field strength at the time of the sudden commencement, other changes in magnitude are seen by ISEE 1 and IMP 8. Because the IMP 8 magnetometer is fixed in a ±36 nT range, however, data gaps occur whenever the field magnitude exceeds this range. When weaker fields are present and IMP-8 data are available, the magnetic field at IMP 8 is weaker than at ISEE 1, reflecting its more tailward location. Also both spacecraft tend to show similar time variations. The absence of field fluctuations at ISEE 1 and IMP 8, low plasma fluxes at ISEE 1, and the lack of energetic
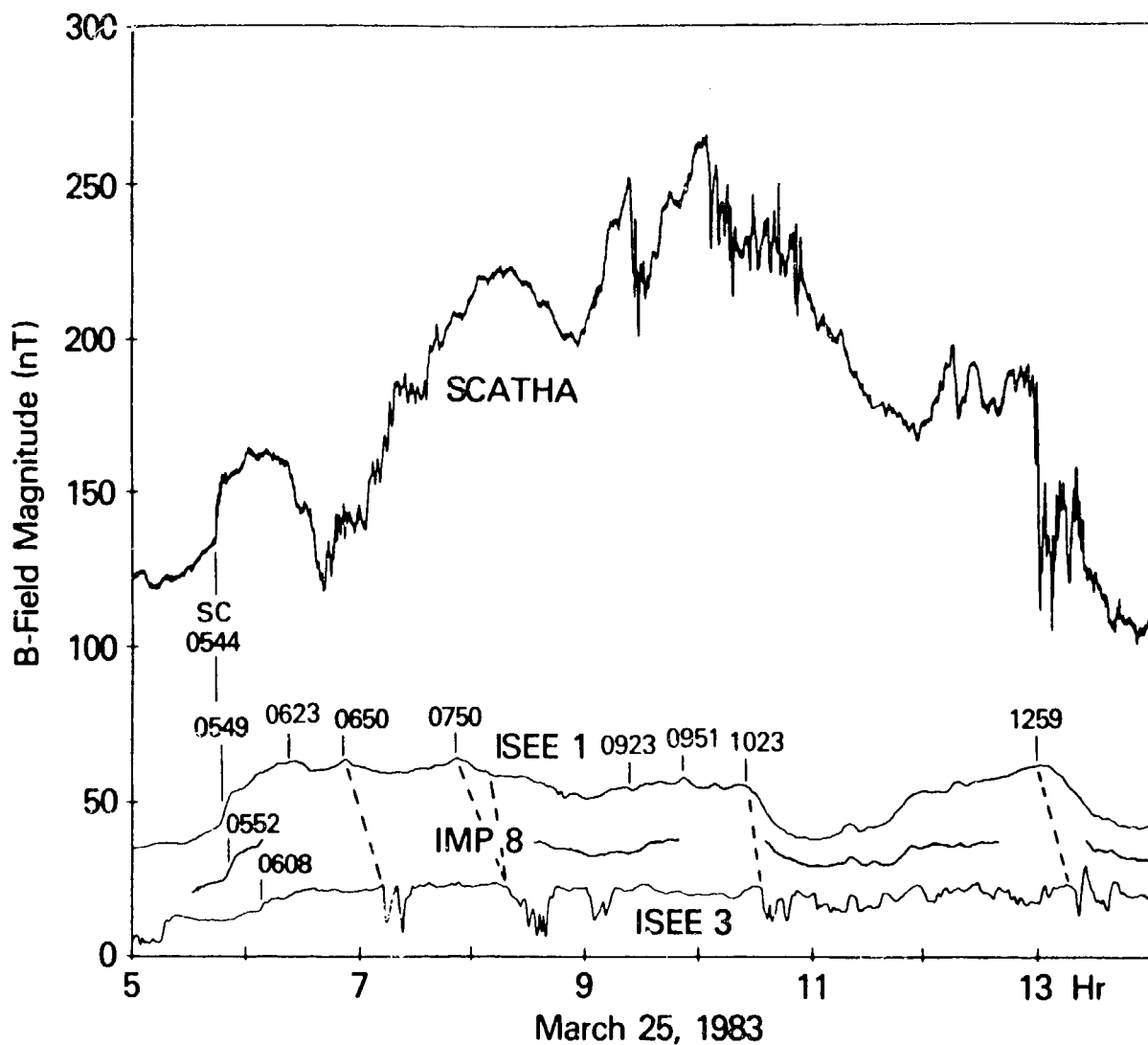
Fig. 4. Magnetic field magnitude measured by SCATHA and the three magnetotail spacecraft. The left most time associated with each trace indicates the arrival time of the sudden-commencement-field compression at the various spacecraft. The remaining times indicate the substorm onset times determined from ground magnetograms and geosynchronous orbit data. Dashed lines indicate the associations between onset times and depressions in the ISEE-3 field magnitude that follow 4 substorm onsets.

particles seen by IMP 8 indicate that these two spacecraft remained continuously in the tail lobe throughout the whole interval. The single exception to this conclusion occurred during a few minute interval near 0850 UT when ISEE 1 briefly entered the plasma sheet.

The variations in field magnitude within the lobe can be related to the substorm intensifications or onsets discussed above on almost a one-to-one basis (See Figure 4). Four of the first five intensifications (except at 0923 UT) are associated with small B decreases. The intensifications at 1023 and 1259 UT, which are the clearest and largest at ground level and those associated with the most intense auroral zone bays, are associated with large decreases in lobe field strength as has often been seen in the past [e. g. Fairfield, 1984 and references therein]. ISEE 1 saw a 31% field decrease from 55 nT to 38 nT between 1020 and 1058 UT, and a 35% decrease from 62 nT to 41 nT between 1259 and 1351 UT.

Variations in the three components of the magnetic field vector at ISEE 1 and IMP 8, and their relation to substorm onsets, are illustrated in Figure 5. The B_z field component at ISEE 1 achieves maximum southward excursions of -8.3 and -9.1 nT near the intensification times of 1023 UT and 1259 UT; the elevation angle of the field relative to the X-Y plane corresponds to almost -9° in each case. This negative component is undoubtedly an manifestation of increased tail flaring prior to the onset. When magnetometer data from IMP 8 resumes after these 2 substorm onsets, the elevation angle for the magnetic field is -13.8° and -6.6° respectively. After each intensification the negative B_z component at each spacecraft increased toward zero. The B_y component at ISEE 1 also increased toward zero thus indicating an overall change toward a more tail-like field with less flaring away from the tail axis.
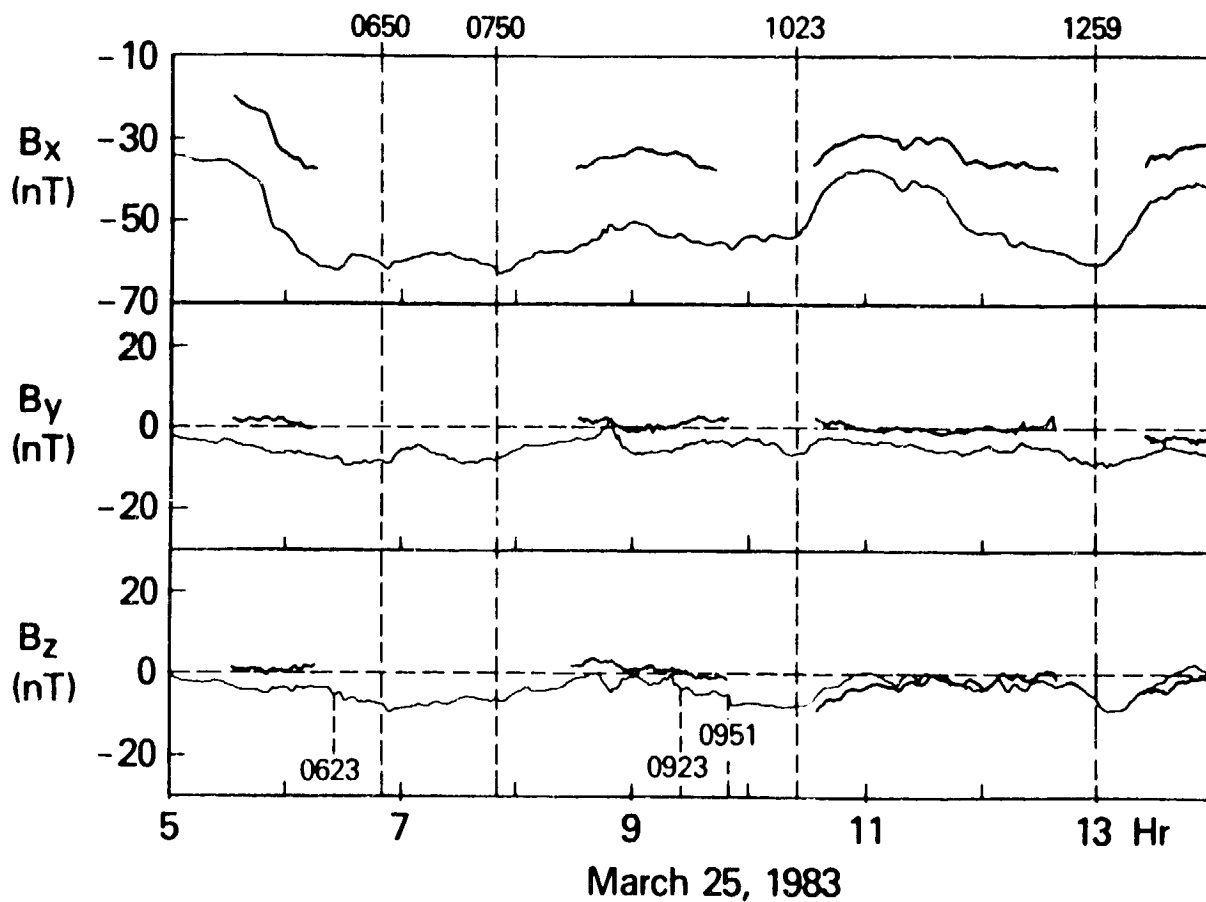
Fig. 5. Magnetic field components at ISEE 1 (continuous trace) and IMP 8 (trace with gaps). The vertical dashed lines indicate the major substorm intensifications associated with large field magnitude decreases and the observation of the plasma sheet at ISEE 3. These 4 intensifications are all followed by increases in the B_z component at ISEE 1 and IMP 8.

We associate the large decreases in field magnitude and the simultaneous variations in field orientation with the onset of the two preceding substorms. This association is based on the facts that (1) such lobe field decreases and B_z increases are commonly observed during substorms [e.g. Fairfield et al., 1981] and are not believed to be due to solar wind pressure changes during the substorms, and that (2) ISEE 3 did not detect any evidence of solar wind pressure changes during the time interval 1100 to 1400 UT when it intermittently crossed into the magnetosheath.

5. POLAR CAP FLUX CHANGES AND TAIL RADIUS

DE 1 spacecraft images are available for 2 of the above substorms so we use this data to estimate changes in the polar cap magnetic flux and the tail radius. Prior to the substorm onset of 1259 UT, DE 1 was outbound toward apogee over the South Pole and was operating in a mode that provided one image of the entire polar region at vacuum-ultraviolet (vuv) wavelength and two images of the dark hemisphere at visible wavelength every twelve minutes. The area of the dark polar cap poleward of the auroral oval and the magnetic flux threading that area are determined from these images. For the present investigation only the images at vuv wavelengths are used. We assume that the flux threading the polar cap is that contained within one lobe of the tail. The area of a cross section of a two-lobe tail in the solar magnetospheric Y-Z plane is then calculated using a circular model of radius R and subtracting a rectangular area representing the plasma sheet. $A_L = \pi R^2 - 2RT$ where T is the full thickness of the plasma sheet [Fairfield, 1986a]. Multiplying half this area by the observed lobe field strength, B_L, we obtain a flux which may be equated to the flux measured simultaneously within the polar cap. Solving for R gives the tail radius as a function of the polar cap flux, the measured field

$$R = \left(T + \sqrt{T^2 + 2\pi F_{pc}/B_L} \right) / \pi$$

Figure 6a illustrates the various quantities discussed above plotted as a function of time during the 1259 substorm. The top trace illustrates how the area of the polar cap indeed decreases during the substorm. The next trace (and that below it from IMP 8) shows that the tail lobe field strength decreases in a similar manner to the polar cap area. This correspondence means that the tail radius at ISEE 1 and IMP 8 distances (shown below B_L) tends to
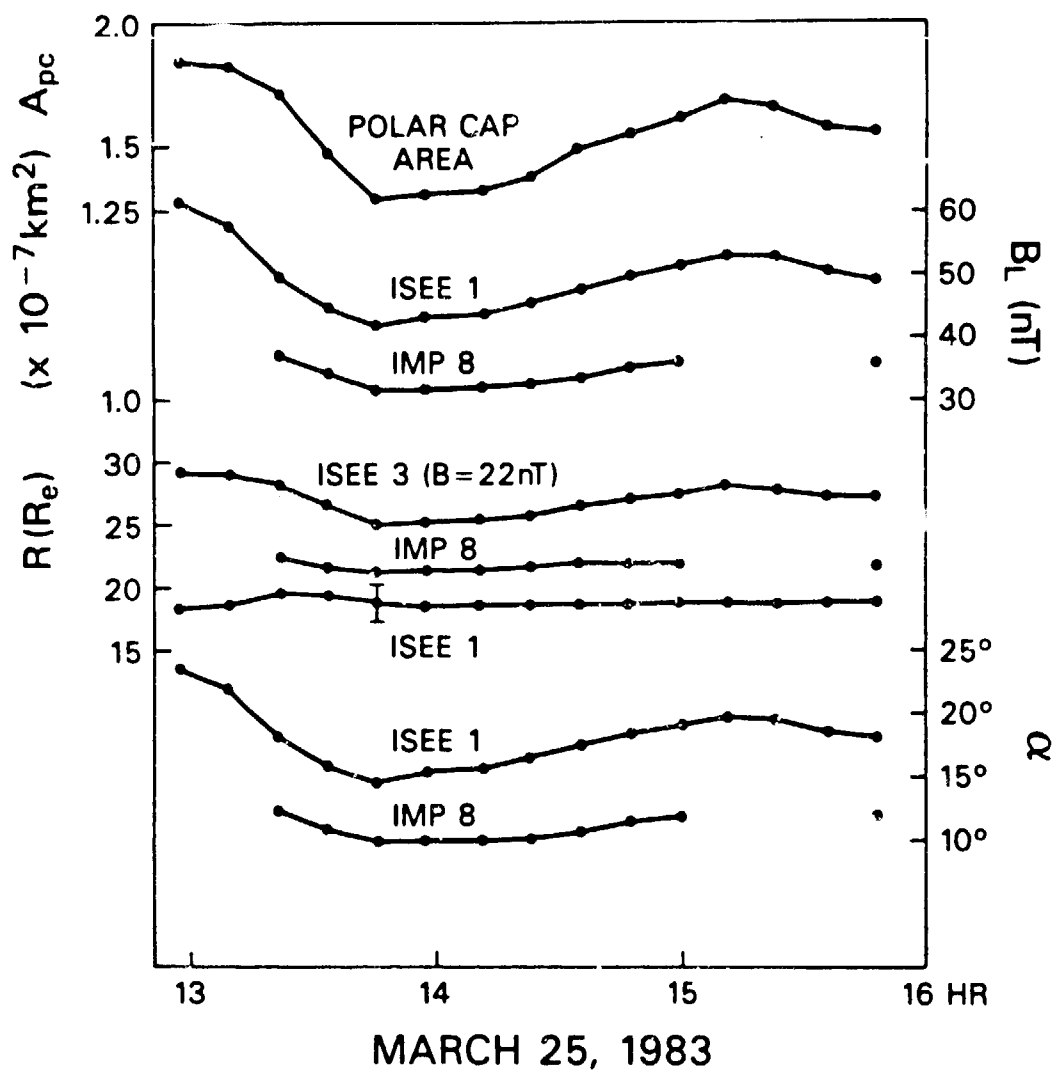
Fig. 6a. Polar cap area determined from DE 1 auroral images is shown by the top trace. Subsequent traces illustrate the tail lobe field strength, B_L, the tail lobe radius determined from the polar cap flux and the tail lobe field strength, R, and the tail flaring angle necessary to produce the observed tail lobe field strength, a.

remain constant. The lobe field strength decreases somewhat more rapidly than the polar cap flux so the radius at ISEE 1 exhibits a slight enhancement near 1330 UT. The radii at all spacecraft are calculated assuming a plasma sheet full thickness (T) of 6 R_E and the upper and lower limits defined by the error bars for ISEE 1 are representative of all spacecraft and correspond to thicknesses of T=10 and 2 R_E, respectively. The radius at ISEE 3 distances is computed by assuming that B_L is a constant equal to 22 nT (see Figure 2) and, hence, changes in radius are due entirely to the measured changes in polar cap area. A second substorm onset occurred beyond the CDAW interval just after 1500 UT and this event is also accompanied by a decrease in polar cap flux and ISEE-1 tail lobe field strength.

DE 1 was also imaging the polar cap following the 0650 substorm and during the 0750 substorm and similar data to Figure 6a are are shown in Figure 6b. The first two polar cap images reveal a decreasing area which probably results from the 0650 onset. The lobe field underwent a relatively small decrease following this onset (see Figure 4). The area then shows a general increase in the 0726-0802 images before beginning a much larger decrease corresponding to the larger tail lobe B decrease following the 0750 onset. It is interesting to note that the geosynchronous spacecraft 1977-007A penetrated the subsolar magnetopause and remained in the magnetosheath from 0655 to 0750 UT, a period which nearly includes the times when the largest lobe fields of the day where measured at ISEE 1 (maxima at 0652 and 0751). The polar cap flux decrease after 0800 is more rapid than the lobe B decrease so that the calculated tail radius in Figure 6 decreases by about 2 R_E in this case.

A second independent determination of tail geometry is obtained by making the assumption that the tail lobe field strength is determined by the component
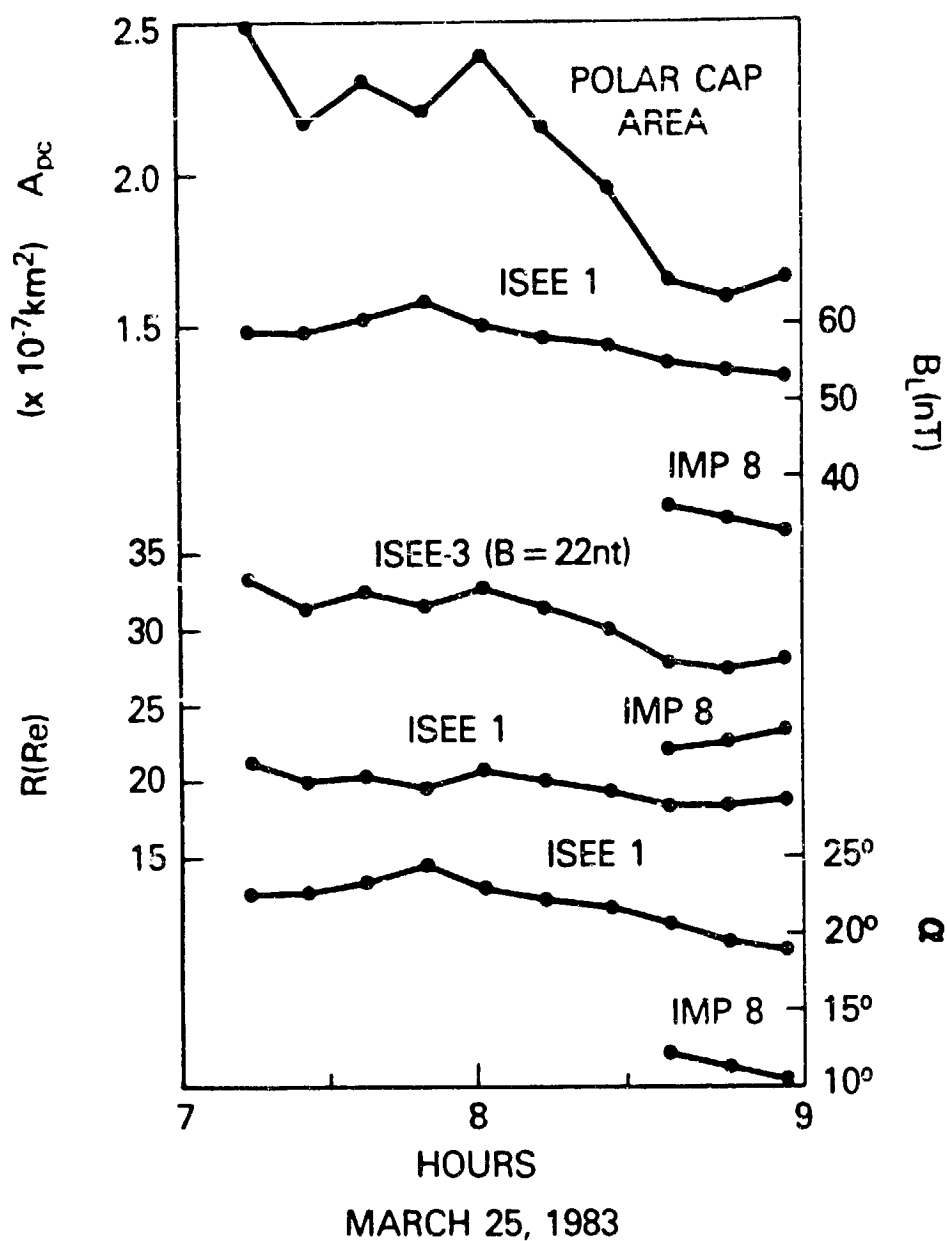
Fig. 6b. Polar cap area and related quantities determined for the 0750 substorm on March 25, 1983. Quantities are identical to Figure 6a.

of solar wind pressure normal to the tail boundary. This assumption is quite good near the subsolar point, but is less accurate on the night side of the earth as the flow becomes more aligned with the boundary [Spreiter and Stahara, 1985]. If the boundary flares away from the tail axis (the solar wind direction) by an angle α and if the external pressure is balanced by the lobe magnetic field strength B_L, then

$$nm_p v^2 \sin^2 \alpha + nk(T_e + T_i) + B_{sw}^2/8\pi = B_L^2/8\pi, \quad (1)$$

where the second and third terms are the thermal and magnetic field pressures of the solar wind. Although we have no direct measure of the interplanetary thermal and field pressure, one can make the assumption that the tail has ceased flaring at the ISEE-3 distance [Slavin et al., 1983; Baker et al., 1984b] so that it is the sum of these unknown pressures that balances the 22 nT lobe field at ISEE 3. Making this assumption one can substitute $B^2/8\pi$ with B=22 nT for the two unknown terms on the left hand side of (1).

If we know the solar wind density and velocity, we can calculate the flaring angle for the distance at which B_L is measured. Although these solar wind parameters are not measured on March 25, we have two indirect indicators of the solar wind pressure. There were the occasional ISEE 3 measurements in the magnetosheath between 1100 and 1400 UT and there is the knowledge cited above that a geosynchronous spacecraft remained within the subsolar magnetosheath for nearly one hour on this day. Quite a large solar wind pressure of $P=3.5 \times 10^{-7}$ dynes/cm^2 must compress the magnetopause to 6.6 R_E (using the normalization of Fairfield, [1979]) but this calculation ignores the observations that show that a southward interplanetary field moves the magnetopause earthward for any given solar wind pressure. The above pressure is equivalent to, for instance, $n \simeq 60$/cc and $v \simeq 600$ km/s, whereas the ISEE-3

magnetosheath measurements after 1100 UT suggest smaller values of $n \simeq 15$/cc and v=550 km/s. We assume the solar wind density and/or velocity have decreased between 0750 and 1300 UT and we use n=20/cc, v=550 km/s (P=1x10^{-7} dynes/cc) for the purposes of computing the flaring angles. The flaring angles are shown by the bottom two traces in Figure 6 for the ISEE-1 and IMP-8 measurements of B_L.

These flaring angles are used when creating the cross-sectional view of the magnetopause shown in Figure 7. The 23° and 15° flaring angles corresponding to the maximum and minimum lobe field strengths observed at ISEE 1 during the 1259 substorm are used to construct tangents to the magnetopause at X=-19.5 R_E (the ISEE-1 distance) and Y=18.5 R_E (the computed tail radius). An 11.5° flaring angle is drawn at X=-30.5 R_E (the IMP 8 distance) and Y=-21 R_E (the IMP-8 tail radius) corresponding to the minimum observed field strength. Two reasonable magnetopause traces are sketched using the above information. An average magnetopause [Fairfield, 1971] is shown by the trace most distant from the earth. For the lobe field minimum, a fairly conventional magnetopause can be drawn (dashed line) with a shape closely resembling the average magnetopause. A much more extremely flared magnetopause must be drawn for the lobe-field-maximum time (solid line). If the 23° flaring angle did not increase further at more earthward distances between X=-19.5 and X=0 R_E, the magnetopause would intersect the Y axis at X=0 at a distance of only 10 R_E. In reality the flaring angle undoubtedly does increase at the more earthward X distances to produce the increasing field values, suggesting that the magnetopause is even closer to the earth than 10 R_E in the dawn-dusk meridian. Such a close in magnetopause is unrealistic, so it is probably appropriate to question the validity of equation 1 in calculating the flaring angle during growth phase conditions.
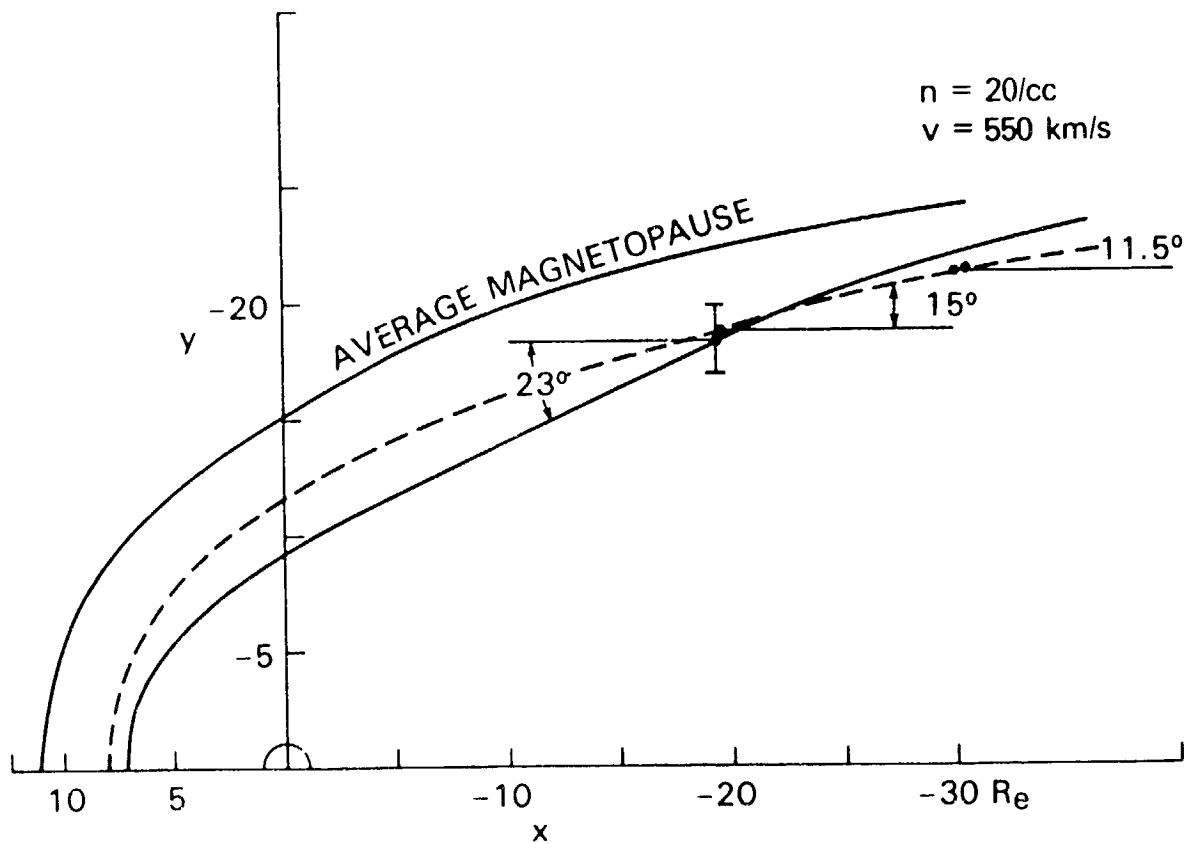
Fig. 7. Illustrating plausible magnetopause shapes that correspond to the tail radii and flaring angles shown in figure 5. The inner solid line represents the pre-onset magnetopause with a large flaring angle and more earthward subsolar magnetopause. The dashed line represents the less flared tail boundary and more distant subsolar magnetopause characteristic of a late phase of the substorm. The outermost magnetopause trace is an average magnetopause characteristic of non-storm conditions [Fairfield, 1971].

33

Before questioning this theory, however, we investigate the uncertainties in these boundary determinations and the possibility that the calculated flaring angle could be smaller. First of all, use of a greater plasma sheet thickness would increase the calculated tail radius and allow for more of an increase in the flaring angle on approaching the earth. The evidence, however, is that the near-earth plasma sheet thins as the magnetosphere becomes more stressed prior to a substorm so this is probably not a plausible alternative. Secondly, one can reduce the flaring by assuming a greater solar wind pressure. This, however, increases the discrepancy with the ISEE-3 measurements of n and v in the magnetosheath. Also, using a higher solar wind pressure creates an increasing discrepancy between the flaring angle and the calculated tail radius change between ISEE 1 and IMP 8; ΔR is the change in radius between ISEE 1 and IMP 8 and ΔX is the position difference, the average flaring angle between the two should be $\alpha \simeq \tan^{-1} \Delta R / \Delta X$. Since ΔX is 11 R_E and ΔR in Figure 6 is approximately 2.5 R_E throughout the event, $\alpha \simeq 13°$. This value is consistent with our choice of n=20/cc, v=550 km/s and in fact was a factor in choosing these values; a higher pressure leads to a value that is too small. Hence it appears difficult to obtain a smaller flaring angle and one must realize that the conventional pressure balance theory predicts a tail flaring angle that is slightly larger than it should be.

Dispite any uncertainties in the theory at small flaring angles it is difficult to avoid the conclusion that (1) the magnetopause is quite drastically flared near substorm onset and (2) the tail radius does not change appreciably during the substorm at $X \simeq -20$ R_E. Maezawa [1975] using Explorer 33 and 35 measurements has shown that after substorm onsets the tail radius does decrease tailward of 20 R_E [see also Baker et al., 1984b; 1987] but this is not

necessarily in conflict with the tail radius being constant near 20 R_E. In fact Figure 7 demonstrates how a stressed (extremely flaring) magnetotail can have a relatively small radius earthward of 20 R_E and a relatively large radius tailward of 20 R_E. If a substorm is due to reconnection at a neutral line near 20 R_E, the radius will decrease tailward of 20 R_E as reconnected field lines escape downstream. The radius will increase earthward of 20 R_E as additional closed field lines move earthward. An increase in the number of closed field lines near the earth increases the thickness of the near earth plasma sheet, as is known to occur. In the model, this would create a larger T which would lead to a greater R even though the polar cap flux and tail field strength might both be decreasing.

6. DISTANT TAIL OBSERVATIONS

Data from ISEE 3 110 R_E downtail are shown in Figure 8. The top panel shows the ISEE-3 magnetic field strength, B, and the energetic ion density, n_{ei}, from the ESA/Imperial College/SRL Utrecht energetic particle anisotropy spectrometer (EPAS). Below are the thermal plasma electron density (n_e) and velocity (V) from the LANL instrument. The energetic particles are associated with plasma-sheet-like regions of weak field and streaming plasma which commence at 0713, 0819, 0902, 1033, and 1318 UT and are marked by vertical dashed lines in Figure 8. Except for the 0902 encounter which is related to the spacecraft return to the northern hemisphere as will be discussed below, all the intervals are associated with preceding substorm onsets as indicated by the times at the top of Figure 8 and dashed lines connecting the ISEE 1 and ISEE 3 traces in Figure 4.

High resolution details of the post substorm encounters with the plasma sheet are shown in Figures 9a-d. In each figure the top three pairs of panels display the electron heat flux magnitude and azimuthal angle, the electron density and temperature, and the flow speed and azimuth, all determined by the LANL plasma electron experiment. Each measurement is completed in one 3 s spin and read out every twelve seconds [Bame et al., 1983]. The electron densities are calculated by numerically integrating over the measured energy range (<1 keV). When the electron temperature exceeds ~10^6°K, part of the distribution falls above 1 keV which results in an underestimate of the actual electron density and temperature. In calculating the heat flux in hot plasma regions, the higher values of the distribution function at the largest measured velocities contribute strongly to the heat flux integral since this integral is weighted by the velocity cubed. In some cases the direction of the heat flux
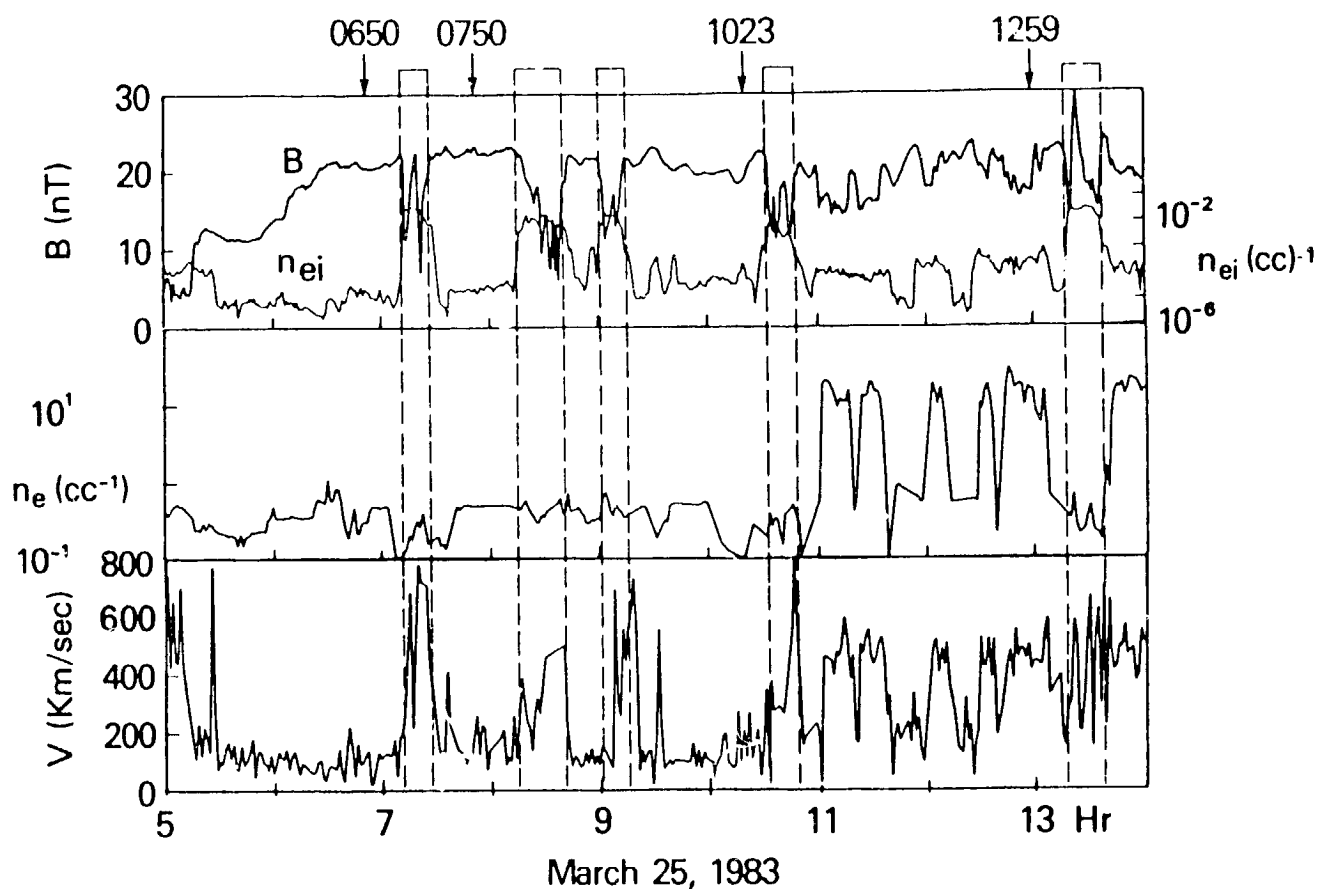
Fig. 8. ISEE 3 measurements in the deep tail on March 25, 1983. Vertical dashed lines bracket plasma sheet intervals with low magnetic field strength, B, high energetic particle density, n_{ei}, and high velocities, V, calculated from the thermal electron experiment. Intervals when ISEE 3 was in the magnetosheath between 1100 and 1400 UT are identified by their high thermal electron densities, n_e, and velocities near 500 km/s.

HEAT FLUX

Log Q

HEAT FLUX AZIMUTH

φ (Deg)

DENSITY

Log N (cm-3)

TEMPERATURE

Log T (K)

FLOW SPEED

V (Km/Sec)

FLOW AZIMUTH

φ (Deg)

MAGNITUDE

B (nT)

Bz (nT)

Bz

AZIMUTH

Φ (Deg)

POLAR

θ (Deg)

0700 0710 0720 0730 0740 0750 0800

ISEE 3 (GSM COORD) 03-25-83
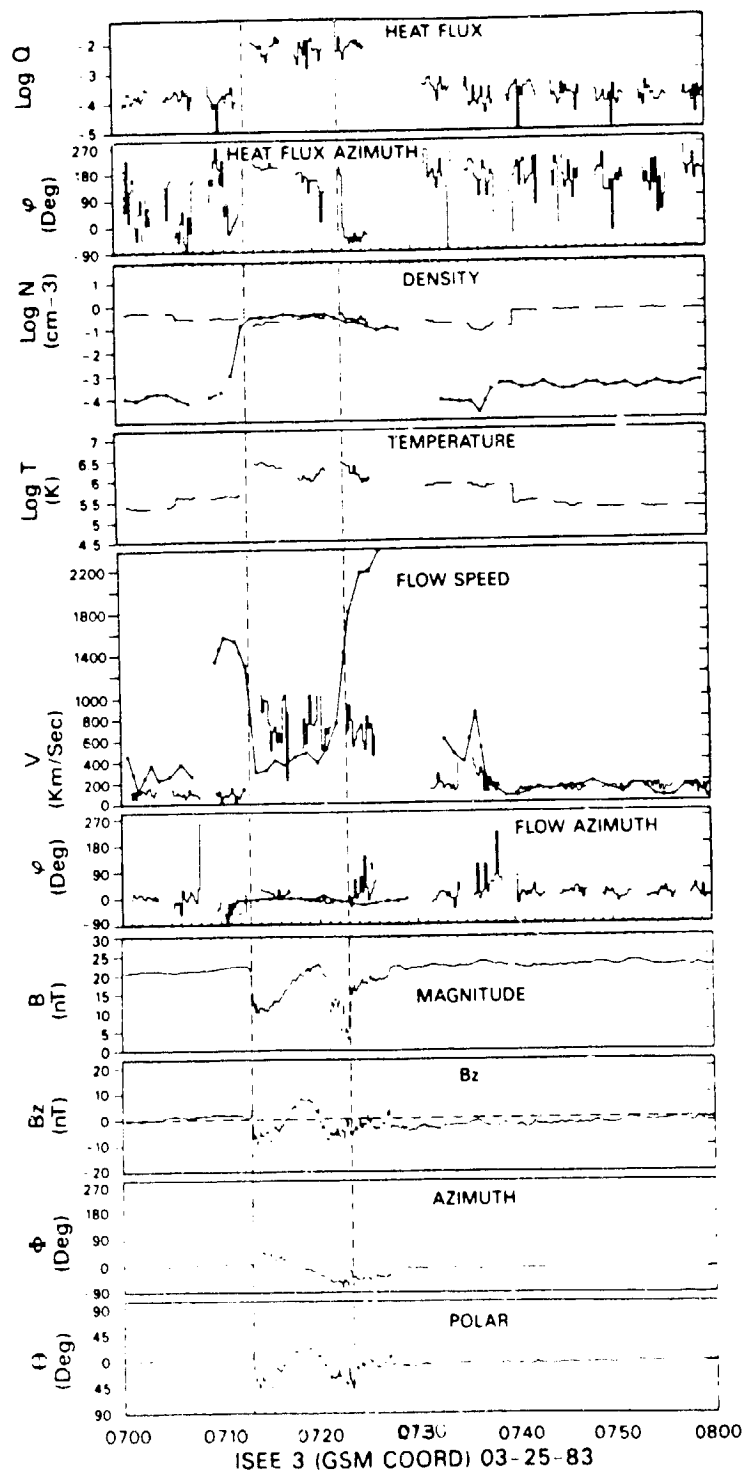
Fig. 9a. High resolution ISEE 3 data from 3 experiments. Twelve second resolution thermal electron data can be recognized by its occurrence in 160 second blocks separated by 80 s gaps. Thermal electron heat flux magnitude and direction, density, temperature, and velocity magnitude and direction are shown in the upper panels. Energetic ion density, flow speed and direction are superimposed with points at 64 s resolution. Lower panels show the magnetic field magnitude, B_z component and azimuthal and polar angles in solar magnetospheric coordinates. Vertical dashed lines span a region of plasma sheet plasma characterized by low field magnitudes with variable direction, high energetic particle density, and high thermal electron density and heat flux. The boundary layer region adjacent to the plasma sheet is characterized primarily by free streaming energetic ions which lead to very high tailward flow speeds. Also elevated electron temperatures and heat flux continue into the region following the plasma sheet.
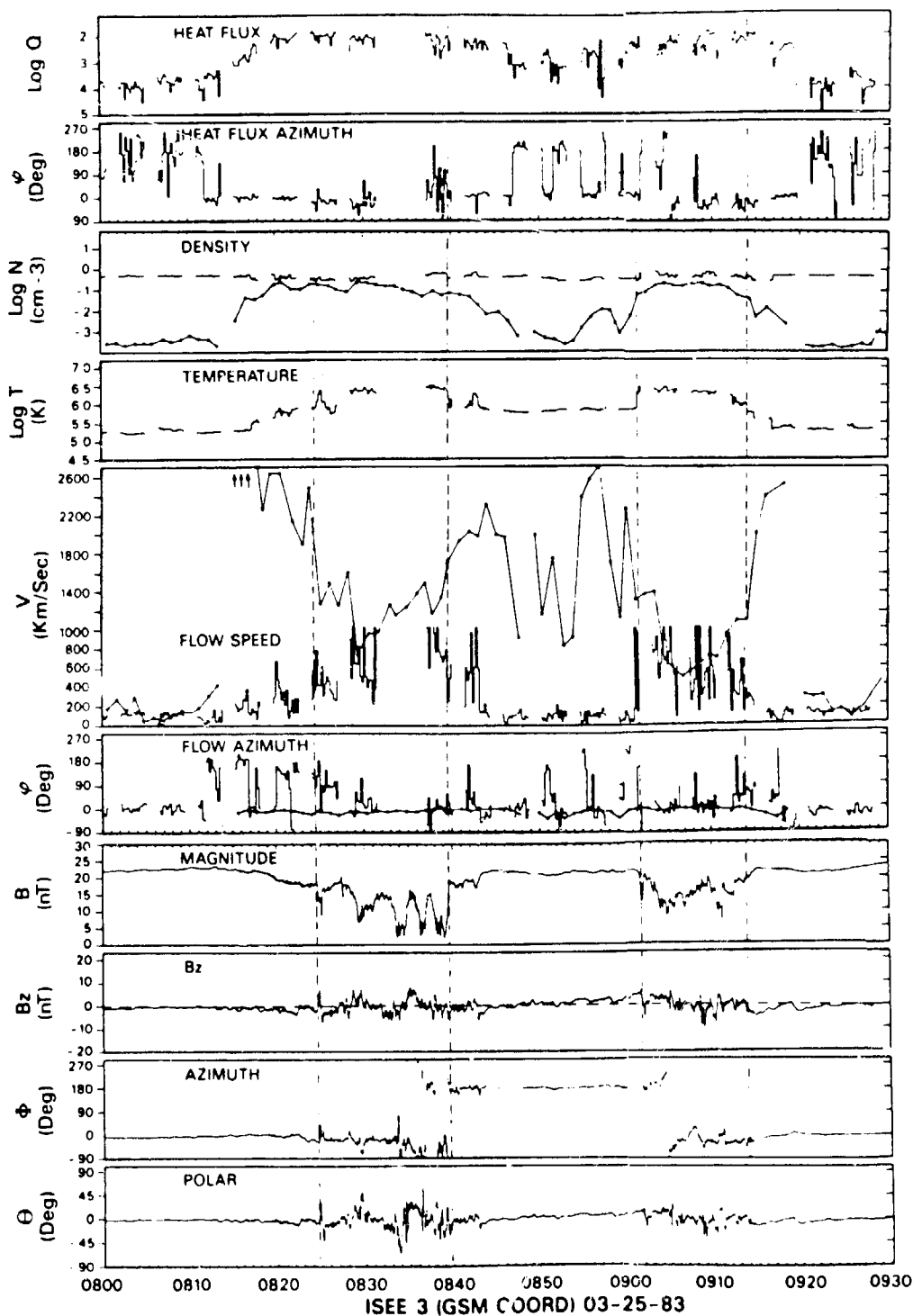
Fig. 9b. A second interval of ISEE 3 plasma sheet plasma in the same format as figure 9a. Tail motion causes ISEE 3 to pass from the northern lobe through the plasma sheet into the south lobe at 0843 before returning back through the plasma sheet into the north lobe at 0914. High tailward flow velocities are detected by both particle instruments within the plasma sheet but the free-streaming, energetic ions produce even higher velocities in the adjacent boundary layer regions.

40
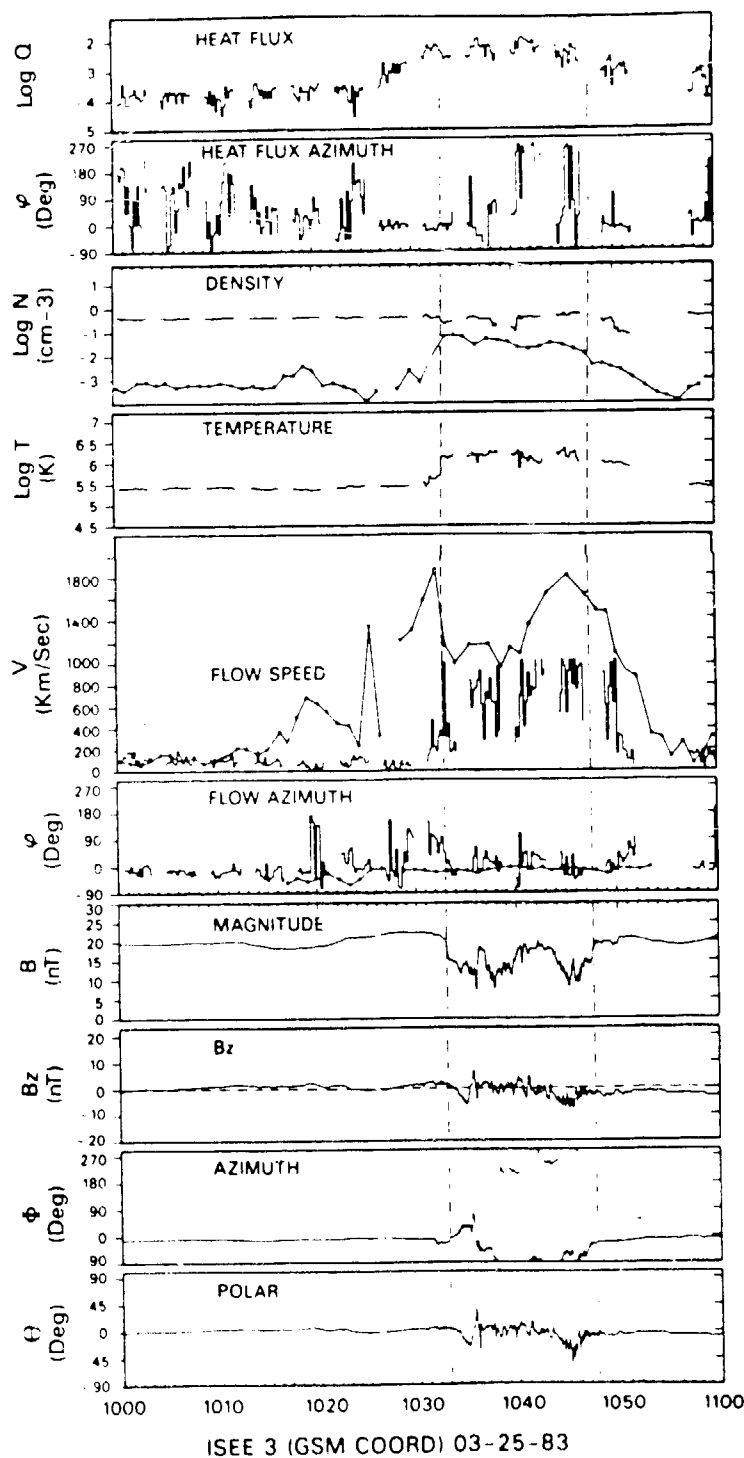
Fig. 9c. A third interval of ISEE 3 plasma sheet plasma in the same format as figure 9a. Enhanced electron temperatures, heat fluxes and energetic ion densities again characterize the plasma sheet but they extend into the adjacent boundary layer regions where the field is more lobe-like.

41
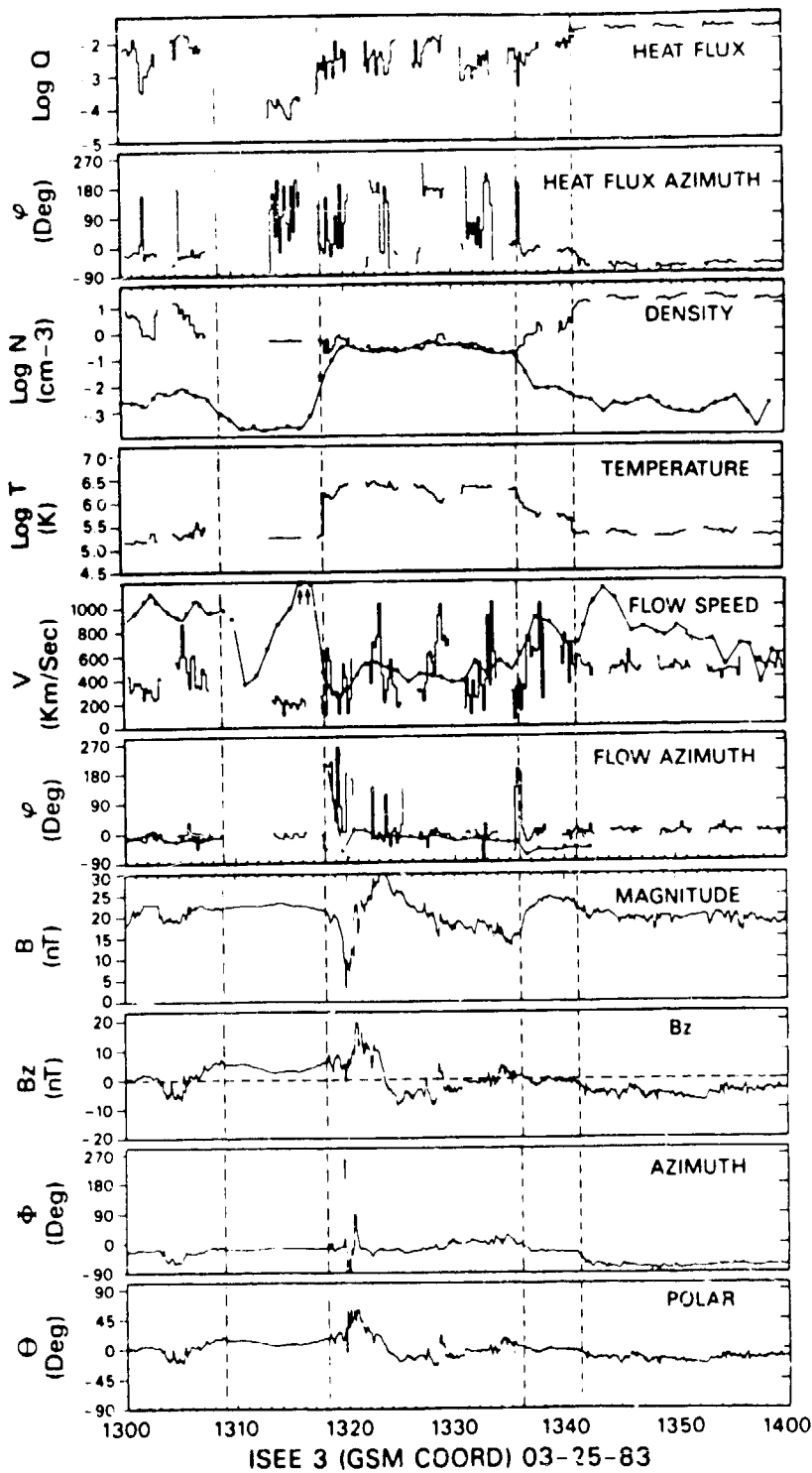
Fig. 8d. A fourth interval of ISEE 3 plasma sheet plasma in the same format as figure 9d. The inner pair of vertical dashed lines denote the plasma sheet region while the outer pair of lines separate preceding and following intervals when ISEE 3 measuring high densities characteristic of the magnetosheath or magnetosphere boundary layer. The north-south B_z transition in the plasma sheet at 1323 is associated with a B magnitude peak as is characteristic of many plasmoids.

42

may be determined by a very small anisotropy which may be unreliable. The energetic ion density and bulk flow speed from the EPAS experiment are overlayed on the electron density and velocity at a resolution of one point every 64s. The EPAS energetic ion densities are calculated using a Maxwellian fit to the measurements which are made at energies ≥ 35 keV. Since the bulk of the plasma ion density is contained in a second lower-energy maxwellian not measured by EPAS, the computed density is usually much lower than the actual total density and n_{ei} is therefore usually less than n_e. As the temperature increases in the plasma sheet, however, n_e is more and more an underestimate of the total density whereas n_{ei} becomes a better, although still low, determination of the total density. The ion flow speeds are derived from the energetic ion anisotropies observed by EPAS using the method of Richardson et al., [1987].

Figure 9a displays the first occurrence of weak field and plasma sheet-like plasma at ISEE 3 following the substorm onset at 0650. The two vertical lines at 0713 and 0723 UT mark the entry into and exit from the plasma sheet which is characterized by an elevated plasma temperature and depressed field strength. The presence of a central peak in the field intensity near 0719 UT will be discussed below. Adjacent to this region and hence lying on lobe-like field lines adjacent to the plasma sheet is a boundary layer. Prior to entrance to the plasma sheet at 0713 UT the boundary layer is characterized by an increased energetic ion density and a high energetic ion velocity which far exceeds that of the local lobe-like plasma. After exit from the plasma sheet at 0723 UT the boundary layer displays these same energetic ion characteristics but also has a slightly decreased field strength and perturbed direction, a slightly enhanced electron temperature. and an enhanced electron heat flux directed in the

43

tailward direction. (Note that whereas the field azimuthal angle is in conventional solar magnetospheric coordinates with 0° pointing toward the sun, the heat flux and flow azimuthal direction angles are defined with a 180° phase shift such that 0° corresponds to flow from the sun, 90° from dusk, etc.) Within the plasma sheet both the thermal electron velocity and the energetic ion velocity generally lie between 400 and 700 km/s, whereas in the boundary layer the energetic ion "velocity" of >1200 km/s greatly exceeds the thermal electron velocity. Richardson et al. [1987] have shown that this behavior is typical of plasma sheet intervals. They argue that the ions in the plasma sheet participate in bulk flow of the plasma whereas the ions in the plasma sheet boundary layer are freely streaming tailward along open field lines which have been reconnected at a neutral line earthward of the spacecraft. The high velocities derived from the ions then arise solely from the strong anisotropy of these ions and do not in fact represent a true bulk motion of the plasma. In this example the heat flux in the plasma sheet is directed toward the earth whereas the velocity calculated from both experiments is directed down the tail.

This 0713 plasma sheet interval was first studied by Sibeck et al., [1984] who suggested that it might be a magnetic "flux rope". Scholer et al. [1985] and Kennel et al. [1986] supported this interpretation but Richardson et al., [1988] prefer to interpret this interval as a 2-loop plasmoid. This latter judgement is based on (1) an isotropic energetic electron flux within the weak field region, (2) energetic particle measurements which indicate a typical southward entry to and northward exit from the region as is typical of plasmoids and (3) the south-north-south B_z field signature which they interpret as the trailing half of one plasmoid followed by a second plasmoid.

44

Figure 9b illustrates the two intervals of plasma sheet plasma beginning at 0824 and 0902. During this event the magnetotail apparently made a northward excursion that caused ISEE 3 to pass from the northern lobe into the plasma sheet (0824-0840 UT) and then on into the southern hemisphere lobe (0840-0902 UT) and finally back into the northern lobe (0914 UT) via the plasma sheet. Again the plasma velocities derived from electron and energetic ion data agree well in the plasma sheet while free tailward-streaming ions (high ion velocities) and magnetosonic waves [Tsurutani et al., 1985] are present in the plasma sheet boundary layers. For this event a strong tailward-directed electron heat flux is present both in the central region and the adjacent boundary layers. The heat flux follows the field direction quite faithfully as the field makes the north-south hemisphere transition, but the velocities are always tailwards.

These 0824 intervals have been studied by Scholer et al. [1984a], Richardson and Cowley [1985] and Richardson et al., [1988]. The earlier studies identified the initial 0824 interval as a plasmoid but Richardson et al., [1988] now question this identification. This reevaluation is based primarily on (1) the existence of tailward streaming energetic electrons within the weak field region and (2) the relatively weak north-south signatures within the structure as is apparent in Figure 9b. To identify this region as a plasmoid one must argue that a series of small north-south variations occurred in the intervals at 0825, 0828-0835, and 0835-0840.

Figure 9c illustrates another ISEE-3 encounter with plasma sheet-like plasma that follows the 1023 substorm intensification by ten minutes. The north-south field perturbation is unlike a classical plasmoid during this event, but B and B_z are rather similar to the 0720 example of figure 9a. The

azimuthal angle is unlike the earlier event however, perhaps because the spacecraft crossed the current sheet and measured fields with directions characteristic of the southern hemisphere during the interval 1038-1046 UT. Note that during the field reversals the polar angle remained small so the field vector rotated in the X-Y plane. Another direction change occurred so that at the peak in field strength at 1042 UT the field was oriented nearly dawnward in the cross-tail direction. The generally tailward directed enhanced heat flux was again present in an extended interval that included the the boundary layers. The heat flux faithfully followed the field during the field reversals to the southern hemisphere directions except for a 180° reversal to keep it oriented tailward. Throughout these field rotations the plasma velocity remained tailward. This interval is somewhat different from the other intervals in that the high velocities determined from energetic ions occurred within the plasma sheet near 1045 UT as well as in the adjacent boundary layer. Apparently the plasma is flowing faster in this event than in other cases; such flow is consistent with a short delay time following substorm onset (see below).

The final plasma sheet-like interval that occurred 19 minutes after the 1259 UT substorm is shown in Figure 9d. Although this interval occurred in close proximity to the magnetosheath and the magnetospheric boundary layer, which was seen before 1306 and after 1341 UT, it displays many features of the earlier events and classical plasmoids. The field strength becomes quite weak at 1320 UT and a very brief excursion to the southern hemisphere is suggested. After this interval the field remains near the X-Z plane and exhibits a large north then south excursion characteristic of a plasmoid. Associated with the north-south reversal is a 30-nT peak in B that is at least 6 nT larger than any

value the adjacent lobe field ever attains. Neither the electron temperature or density show a decrease at the time of this field peak nor does a detailed examination of the electrons reveal a departure from plasma sheet-like spectra. These facts indicate that the peak definitely occurs within the plasma sheet and suggest a lack of pressure equilibrium at this time. Tailward convecting plasma is confined to the plasma sheet between the inner pair of vertical dashed lines. Higher energetic particle velocities due to particle streaming occur in the adjacent boundary layers and tailward heat flux occurs in the trailing boundary layer. Although the heat flux is somewhat weaker in the plasma sheet-like region compared to earlier events, the strongest interval of heat flux at 1328 is associated with a cooler, denser plasma and it is directed in the earthward direction. This event appears to be the clearest plasmoid event on this day (see also Richardson et al., [1988]).

If the events of Figures 9a-d are to be interpreted as plasmoids, it is important to estimate their sizes and their arrival times at ISEE 3 reative to sustorm onset times. The first 3 columns of Table 2 list the onset time at ISEE 3 of the 4 plasma sheet intervals, the onset time of the associated substorm near earth, and the difference between these times. Following the 0750 onset we list the alternative 0807 time discussed above whose use is necessary to obtain reasonable velocities. The measured plasma velocities are displayed in column 4 which gives a range of velocities which roughly bracket the velocities from the two instruments. Column 5 lists the duration of the plasma sheet interval with the duration of the plasmoid interval in parenthesis.

For the event in Figure 9a we assume, following Richardson et al. [1988], that the first of two plasmoids arrived 3 minutes before the spacecraft moved into the weak field region and hence the leading half was was not detected by

47

Table 2. Transit to ISSE 3

Plasma Sheet Onset Time	Substorm Onset Time	Transit Time (m)	Measured Plasma Vel.	Duration ΔT (m)	L (R_E)	Transit Vel. (km/s)
0713	0650	23	400-700	10 (6)	31	310
0824	0750(0807)	34(17)	800-1200	15 (1.5)	14	480
1033	1023	10	900-1400	15 (5)	54	510
1318	1259	19	300-600	18 (10)	42	270

the spacecraft. It is then concluded that the plasmoid duration is 6 m. Multiplying this duration by the midpoint velocity from column 4 gives a plasmoid length of 31 R_E as is shown in column 6. The 0824 event in figure 9b involves a high measured velocity and is complicated by the transverse motion of the tail that moves the spacecraft from the north to south lobes. This event is the most difficult to reconcile with the plasmoid model and in fact Richardson et al. [1988] argue that it is not a plasmoid. If, however, we focus on a very brief north-south B_z variation at 0825 with duration 90 s we can obtain a plasmoid of lenght 14 R_E. For the 1033 event we again assume that only the trailing half of a 5 minute plasmoid was detected, giving a 54 R_E plasmoid. For the last event we consider the plasmoid as the first 10 minutes of the interval where the classical north-south B_z is observed. This event also yields a length of 42 R_E. Note that the portion of this plasma sheet interval following the plasmoids in figues 9c and 9d has the predominantly southward field characteristic of the post-plasmoid plasma sheet discussed by Richardson and Cowley [1985]. The plasma sheet following the plasmoids in Figures 9a (and perhaps 9b) has a second plasmoid.

Finally we assume that the plasmoids are released from 20 R_E at substorm onset time. Dividing the distance 90 R_E minus the plasmoid length by the transit time in column 3 (and accounting for the unseen earlier arrival before 0713 and 1033) we obtain an average transit velocity shown in column 7. In all

cases this average transit velocity is less than the measured "final" velocity. This difference can be interpreted as evidence for acceleration of the plasmoid from zero velocity so that the average value that is calculated is less than the final velocity that is measured.

Another characteristic of at least three of the four plasma sheet events (Figures 9a,c and d) is a field magnitude peak within the weak field region. This feature is not a previously reported feature of plasmoids and is contrary to the simple plasmoid model with an "O" type neutral line at the center of a flux loop, at least if the spacecraft is passing anywhere near this weak field region. However, examination of both published and unpublished examples of pla 'oids reveals that such a field peak is in fact a feature of the majority of plasmoids [e.g. Baker et al., 1987, figures 4,5 and 6; Richardson et al., 1987, figures 3 and 4; see also Slavin et al., 1988]. In these examples the peak is invariably associated with any north-south B_z transition in the manner illustrated especially clearly by Figure 9d.

Two explanations of this high field peak seem possible. Slavin et al., [1988] propose an explanation that is essentially that used to explain traveling compression regions [Slavin et al., 1984]. This explanation states that the field within the closed plasmoid loop and north or south of the "O" line of the locp will b~ compressed by the enhanced pressure caused by the passing plasmoid. This compression is less important near the ends of the plasmoid so that a weak field region will be seen on either side of the peak. This explanation implies that the peak will be absent if the spacecraft passes near the "O" line but it will have maximum amplitude if it passes near the northern or southern boundaries of the plasmoid. As mentioned above, however, the thermal electron data at the time of the 1323 peak does not reveal any

49

decrease in plasma pressure as one might expect if plasma were being squeezed out of the region.

A second alternative explanation of the field magnitude peak is that of a flux rope. In this case a strong axial field at the center of the flux rope would provide a natural explanation of the peak if the spacecraft moves directly through the structure. This in fact was Sibeck et al.'s [1984] original explanation for the 1033 event although recent evidence [Richardson et al., 1988] now suggests that such uniform motion did not occur. It seems that the flux rope model, and in particular a theoretically interesting force-free equilibrium model with constant pitch of the field [e.g. Burlaga, 1988], might well explain both the observed magnitude and angular variations. The problem with this explanation is that such a flux rope would be approximately oriented along the tail axis in figures 9a and 9d, and it is difficult to reconcile such an orientation with the observed motion and time delays that are more easily explained by the plasmoid model.

Another feature not readily reconciled with the classical plasmoid picture is the existence of strong heat flux in the plasmoid-like regions if indeed the measurements represent a true heat flux. Closed flux loops might support a bi-directional electron anisotropy but such loops would be detached from any heat source which would seem to preclude a strong heat flux. In fact a close examination of electron distributions sometimes reveals evidence for such a bi-directional anisotropy along with the evidence for a heat flux. A true heat flux is probably more compatible with the flux rope explanation.

at a location only 7° west of GOES 5. This event had little effect on particles measured by 1981-025B in the region just before midnight. The data are missing at GOES 2.

Pi2 pulsations and magnetogram component changes indicated that the next important intensification occurred at 0750 UT. Positive B_y perturbations occurred at Newport (Figure 10) and Lompoc (Figure 3), and negative B_y perturbations occurred at Rapid City, Camp Douglas, Mt Clemens (Figure 10) and Boulder (Figure 3). Positive H bays were seen at Rapid City, Newport, (Figure 10) Tucson and Boulder and slightly later at Lompoc (Figure 3). The auroral electrojet was apparently near Meanook judging from a large sharp negative B_x perturbation at 0750 that was accompanied by little B_z perturbation. These observations place the onset near 310° longitude or very near local midnight. A field dipolarization was detected by GOES 2 at 0753 UT near 0100 LT but not at GOES 5 near 0300 LT. At 2300 LT, intense fluxes of energetic electrons at 1981-025B increased even more at 0759 UT and the field angle computed from the electron anisotropy (not shown) [Baker et al., 1981] also increased. At 0300 LT spacecraft 1982-019A detected a brief electron increase at 0800 UT that was superimposed on a decreasing trend. Further variations of magnetograms in the subsequent half hour suggest the possibility of further intensifications, but it is difficult to distinguish spatial motion of current systems from time changes in intensity during this complicated interval.

A rather minor intensification occurred at a time which is tentatively placed at 0923 UT. The event was apparently centered near 0100 LT as deduced from positive B_y at Victoria (not shown) and Newport and negative B_y's at Rapid City and stations to the east along with positive H bays at Boulder, Tucson, Lompoc, Rapid City and Newport. Little evidence was seen for the auroral
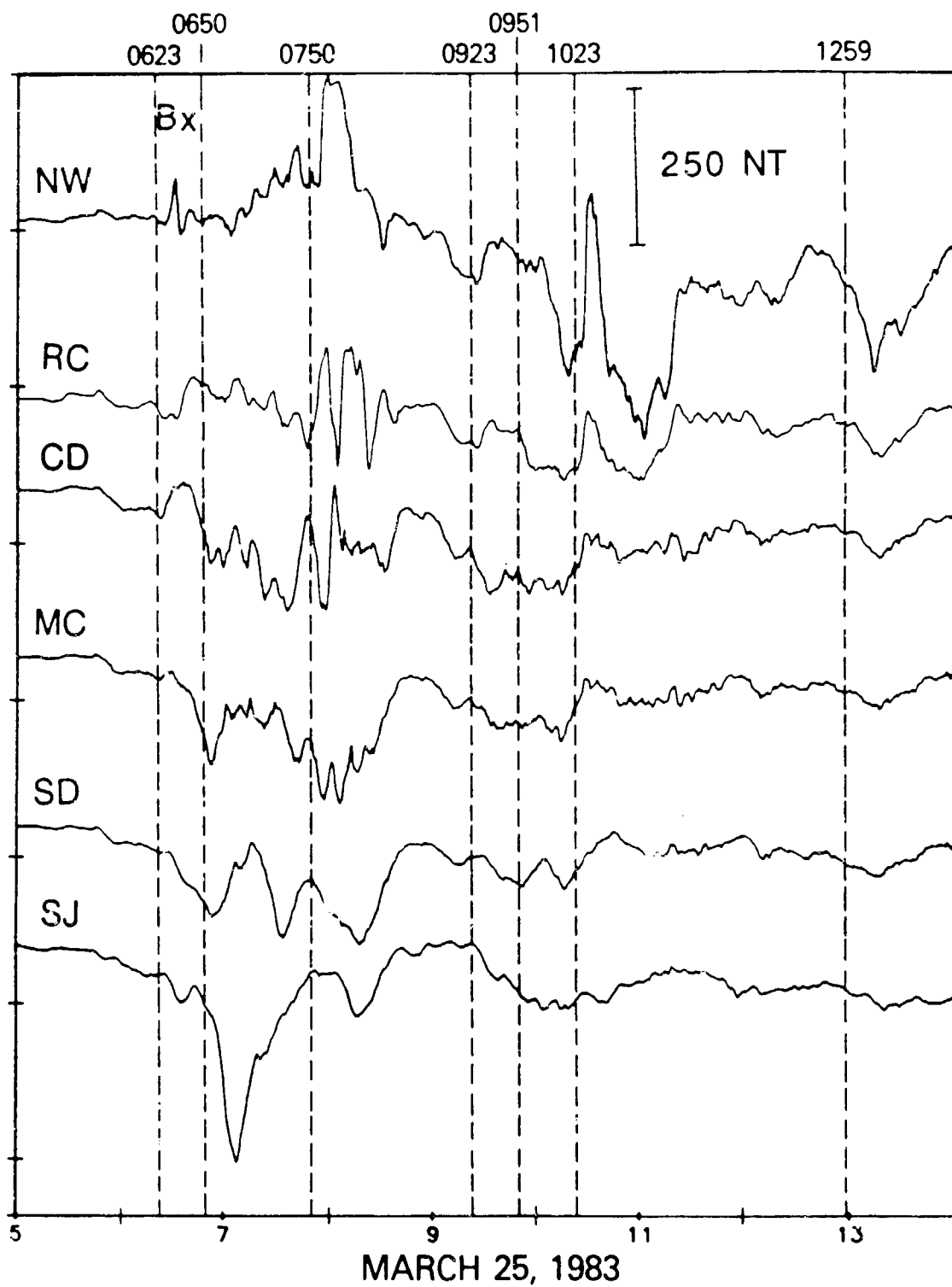
51

Fig. 10a. B_x component magnetograms from the AFGL longitudinal chain of observatories.
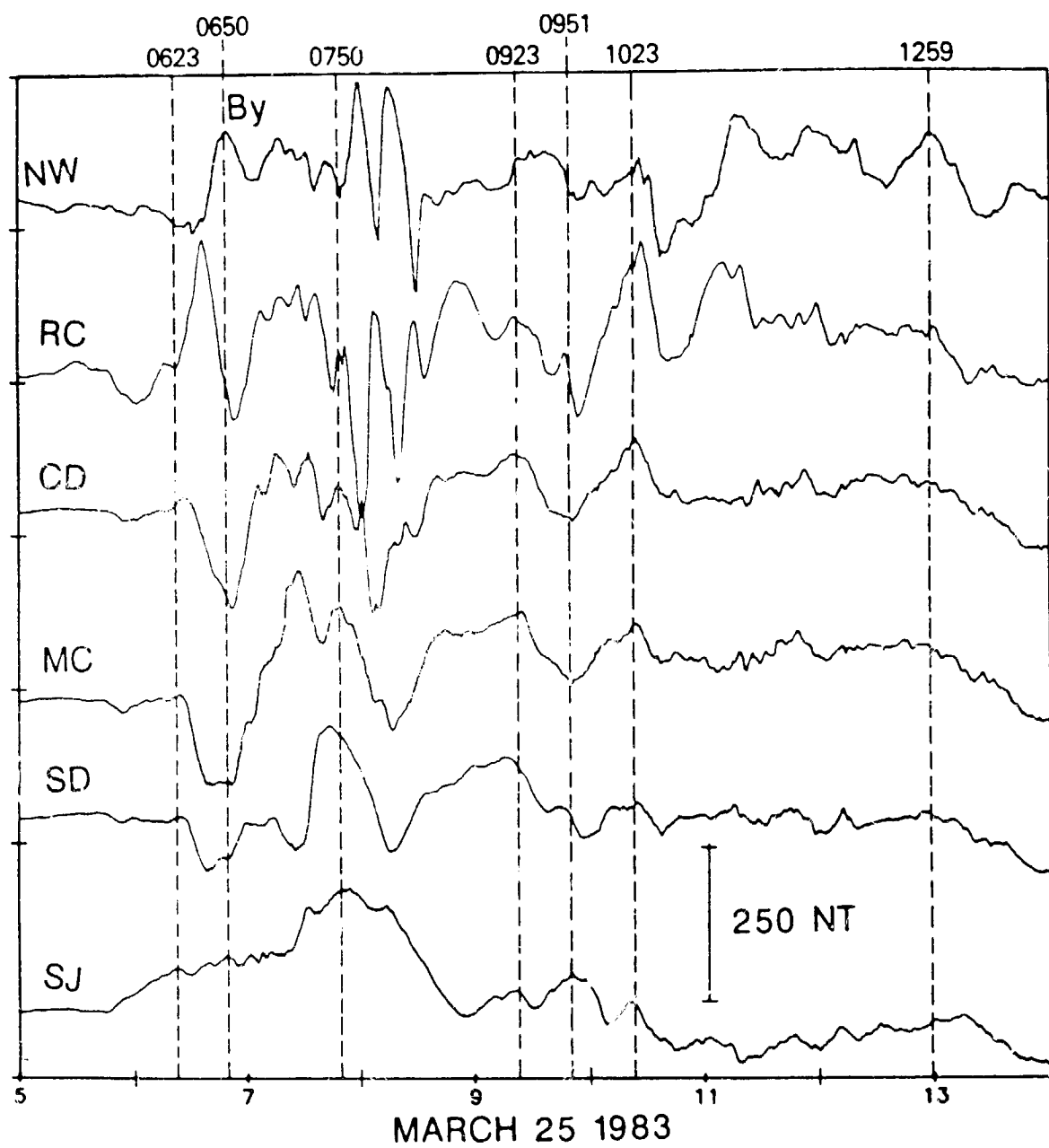
Fig. 10b. Same as figure 10a for the B_y magnetogram components.

electrojet although there was a large negative B_y perturbation at Barrow. GOES 2 (0230 LT) saw a small dipolarization beginning at 0923 and spacecraft 1981-025B saw a small increase in energetic protons at 0928 UT. Scatha at 1930 LT saw a particle increase and a small dipolarization but this may be unrelated to the event near midnight at such an early local time.

Another intensification was marked by positive B_y perturbations at Mt Clemens, Camp Douglas at 0951 and at Rapid City, Boulder and Tucson further to the west a few minutes later. Negative By occurred at San Juan (not shown) and Sudbury; these negative perturbations were more gradual but occurred at an earlier time of about 0946. Positive bays occurred at Fredricksburg and San Juan (not shown) and Sudbury at 0951. This event therefore appeared to be centered near 350° which places it at the unusual location of 0400 LT. These ground observations are supported by the satellite data. GOES 5 near 0500 LT detected a theta increase at 0946 UT but GOES 2 near 0300 observed only a small increase near this time. Spacecraft 1981-025B near the 0100 LT observed electron and ion increases at 0949 UT. Spacecraft 1982-019A detected a large increase in electrons and ions but not until 0959 UT (0500 LT).

A very significant intensification occurred at 1023 UT. Most midlatitude stations within North America detected negative By perturbations with the stations more to the west exhibiting the reversal from the earlier positive perturbation at a somewhat later time. The likely local time of the current wedge center would appear to be near the west coast of North America or near 0200 LT. This event in contrast to the intensifications during the previous 2 hours, produced very large negative bays at the stations above 64° geomagnetic latitude. Onset times were College 1027 UT, Yellowknife 1025 UT Churchill 1024 UT. There was a small dipolarization at Scatha (2130 LT) at 1019 UT. GOES 2

54

near 0300 LT detected high levels of fluctuations but no clear dipolarization and GOES 5 had moved too far to the east to see any effects. The 1981-025B energetic electrons intensity increased at 1027 UT (0130 LT) and the inferred field angle computed from the electron distributions showed a large increase at the same time. Energetic electrons at spacecraft 1982-019A also showed an increase at 1030 UT even though this spacecraft had almost reached the dawn meridian.

By 1200 UT the SCATHA spacecraft was approaching the midnight meridian. SCATHA saw a classical stretching of the field [Baker et al., 1981] and disappearance of energetic particles followed by an abrupt dipolarization and particle return at 1259. This large onset produced negative, midlatitude B_y's throughout the North American sector and as far west as Honolulu (not shown). A large positive H at Guam with no B_y perturbation marked this longitude (2200 LT) as near the onset meridian. Large negative H bays are seen at College and Canadian observatories to the east. The other synchronous orbit spacecraft had moved well to the east by this time and saw only delayed particle increases.

In conclusion, we have identified seven times of significant substorm onsets or intensifications as are marked on the figures. It should be appreciated, however that during this complex interval of ongoing activity there are probably other times of increases in field aligned current systems with lesser magnitudes and smaller spatial scales that can effect individual observing points both on the ground and in space. We feel that the seven events are the most reasonable choices for comparisons with data in the deeper magnetotail.

7. SUMMARY AND CONCLUSIONS

Multiple spacecraft data sets of March 25, 1983 have been used to confirm many characteristics of magnetotail dynamics that have been discovered by earlier studies. At the time of a ssc on March 25, a magnetic field compression was observed in succession by four different spacecraft at increasing distances in the tailward direction. The delay times were compatible with the expected delay times for a convected pressure increase associated with an interplanetary shock moving away from the sun.

Two spacecraft in the tail lobes near $X \simeq -20$ and -30 R_E detected magnetic field changes typical of substorms. The tail lobe field strength decreased in association with 6 of 7 substorm onsets or intensifications as determined by ground magnetometers and geosynchronous spacecraft. During the four largest intensifications as determined on the ground, a tail magnetic field reconfiguration at 20 and 30 R_E was indicated by an increase in B_z during the 10's of minutes following the substorm onset. These observations confirm that (1) the tail typically loses energy beginning at the time of substorm onsets and (2) more magnetic flux closes across the equatorial plane after a substorm as would be expected if formerly open field lines had become closed by reconnection.

The changing amount of open flux threading the polar cap during substorms was determined by measuring the size of the dark polar cap on spacecraft images of the aurora. During the two substorms imaged by spacecraft, the polar cap flux decreased by 30 and 36% during the hour following substorm onset. This observation further supports the occurrence of reconnection that converts open tail lobe field lines to closed plasma sheet field lines during substorms.

It was further noted that the tail lobe field strength at 20 R_E tended to decrease in proportion to the polar cap flux decrease following the 1259 onset so that little change in the tail radius near 20 R_E was required to accommodate the time varying open flux. The changing field strength at 20 R_E, however, required a substantial change in tail flaring angle; an extremely flared tail was present before onset that is consistent with a close-in subsolar magnetopause, whereas a less flared magnetotail was present during recovery that must be accompanied by a more distant subsolar magnetopause. This conclusion is consistent with tail flux returning to the dayside during the substorm. The constancy of the tail radius near 20 R_E suggests that this distance is near the "pivot point" around which the boundary "rotates"; the tail radius will reach a maximum at more tailward locations before onset and decrease at such locations during the substorm. Earthward of this pivot point the changes will be in the opposite sense. To create such boundary changes the neutral line probably creates closed flux in the vicinity of 20 R_E for this event. Similar polar cap flux changes occurred following the 0750 (or 0907) substorm, although a slightly larger polar cap change suggested a decrease in the tail radius at $X \simeq -20$ R_E.

In many respects the observations from ISEE 3 at $X \simeq -110$ R_E resemble plasmoids, and therefore support the near earth neutral line model of substorms. The four principle ground onsets that were associated both with major tail lobe reconfigurations and with the largest tail energy losses are also those four events where ISEE 3 detected distinct weak magnetic field regions containing hot plasma-sheet plasma flowing rapidly in the tailward direction. The simple north-south B_z signature characteristic of a single plasmoid was clearly present only for the last of 4 events although multiple

plasmoids could perhaps explain several others. The arrival times are compatible with the plasmoid model once appropriate decisions are made about exactly what constitutes the individual plasmoids. The characteristic plasma sheet behavior and surrounding boundary layer phenomena are characteristic of plasmoids, yet they are typical of almost any plasma sheet entry and hence cannot be considered unique support for plasmoids. The heat flux within the plasmoids seems to argue against the plasmoid picture, yet interpretation of these measurements as a true heat flux may be suspect.

On the other hand, flux ropes may provide an alternative explanation for at least some of the ISEE 3 events. It is not immediately apparent how to reconcile this model with other features more easily explained by plasmoids, but the field signatures appear appear consistent with that expected from a spacecraft moving through such a structure. In an attempt to reconcile the various points of view we suggest the following considerations.

First, the standard plasmoid picture may be basically correct, but the plasmoid may be of limited extent in the Y direction as was found in the 3 dimensional simulations of Birn and Hones [1981]. The edges of the plasmoid might appear different from what is seen nearer the center. The time relation with substorms might still be present but the different and unknown structures on the edges might explain those events that deviate from the standard model.

A second possibility is that the substorm onset may be associated with an increase in the reconnection rate at a preexisting near-earth neutral line, so that no plasmoid is formed but the plasma sheet tailward of the neutral line expands over the spacecraft, as discussed in Richardson et al., [1988]. This suggestion is supported by the slight preference for southward fields in the 0824 and 1033 plasma sheet encounters. Additional field loops within such a

59

region could explain further complexity.

A third possibility is that a plasmoid like structure is released at substorm onset that carries field aligned currents and is similar to a flux rope. Hughes and Sibeck [1987] have suggested such a model whereby a three dimensional flux rope extending across the tail is created by near earth reconnection in the presence of a cross-tail field component. At least one end of this flux rope may break off and convect downstream at the time of substorm onset. In the limit of no B_y component, the model reverts to the simple 2-dimensional plasmoid, current-loop picture. It would appear that this type of 3-dimensional model may ultimately be able to reconcile the different angular variations of the field that is the significant distinguishing difference between plasmoids and flux ropes. It would also be easier to explain enhanced electron heat fluxes with such a three dimensional picture.

REFERENCES

Aubry, M. P., C. T. Russell, and M. G. Kivelson, On inward motion of the magnetopause before a substorm, J. Geophys. Res., 75, 7018-7031,1970.

Baker, D. N., E. W. Hones, Jr., P. R. Higbie, R. D. Belian, and P. Stauning, Global properties of the magnetosphere during a substorm growth phase: A case study, J. Geophys. Res., 86, 8941-8956, 1981.

Baker, D. N., S. J. Bame, R. D. Belian, W. C. Feldman, J. T. Gosling, P. R. Higbie, E. W. Hones, Jr., D. J. McComas, and R. D. Zwickl, Correlated Dynamical Changes in the near-earth and distant magnetotail regions: ISEE 3, J. Geophys. Res., 89, 3855-3864, 1984a.

Baker, D. N., S. -I. Akasofu, W. Baumjohann, J. W. Bieber, D. H. Fairfield, E. W. Hones, Jr., B. H. Mauk, R. L. McPherron, and T. E. Moore, "Substorms in the magnetosphere," Chapter 8 of Solar Terrestrial Physics – Present and Future, NASA Pub. 1120, Washington, D. C., p 8-1 to 8-55, 1984b.

Baker, D. N., R. C. Anderson, R. D. Zwickl and J. A. Slavin, Average plasma and magnetic field variations in the distant magnetotail associated with near-earth substorm effects, J. Geophys. Res., 92, 71-81, 1987.

Bame, S. J., R. C. Anderson, J. R. Asbridge, D. N. Baker, W. C. Feldman, J. T. Gosling, E. W. Hones, Jr., D. J. McComas, and R. D. Zwickl, Plasma regimes in the deep geomagnetic tail: ISEE 3, Geophys. Res. Lett., 10, 912-915, 1983.

Birn, J., and E. W. Hones Jr., Three-dimensional computer modeling of dynamic reconnection in the geomagnetic tail, J. Geophys. Res., 86, 6802-6808, 1981.

Burlaga, L. F., Magnetic clouds and force-free fields with constant α, J. Geophys. Res., 93, In Press, 1988.

Clauer, R. C., and R. L. McPherron, Mapping the local time – universal time developement of magnetospheric substorms using mid-latitude magnetic observatories, J. Geophys. Res., 79, 2811-2820, 1974.

Fairfield D. H., Average and unusual locations of the earth's magnetopause and bow shock, J. Geophy. Res., 76, 6700-6716, 1971.

Fairfield, D. H., Global aspects of the earth's magnetopause, in Magnetospheric Boundary Layers, European Space Agency Scientic and Technical Publications Branch ESA SP-148, p 5-13, Noordwijk, The Netherlands, 1979.

Fairfield, D. H., Magnetotail energy storage and the variability of the magnetotail current sheet, in Magnetic Reconnection in Space and Laboratory Plasmas, E. W. Hones Jr., editor, American Geophysical Union, Washington D. C., 168-177,1984.

Fairfield, D. H., Time variations of the distant magnetotail, Geophys. Res. Lett., 13, 80-83, 1986a.

Fairfield, D. H., The magnetic field of the equatorial magnetotail from 10 to 40 R_E, J. Geophys. Res., 91, 4238-4244, 1986b.

Fairfield, D. H., R. P. Lepping, E. W. Hones Jr., S. J. Bame, and J. R. Asbridge, Simultaneous measurements of magnetotail dynamics by IMP spacecraft, J. Geophys. Res., 86, 1396-1414, 1981.

Holzer, R. E., and J. A. Slavin, Magnetic flux transfer associated with expansions and contractions of the dayside magnetosphere, J. Geophys. Res., 83, 3831-3839, 1978.

Hones, E. W. Jr., Transient phenomena in the magnetotail and their relation to substorms, Space Sci. Rev., 23, 393, 1979.

Hones, E. W. Jr., D. N. Baker, S. J. Bame, W. C. Feldman, J. T. Gosling, D. J. McComas, R. D. Zwickl, J. A. Slavin, E. J. Smith, and B. T. Tsurutani, Structure of the magnetotail at 220 R_E and its response to geomagnetic activity, Geophys. Res. Lett., 11, 5-7, 1984.

Hughes, W. J., and D. G. Sibeck, On the three dimensional structure of plasmoids, Geophys. Res. Lett., 14, 636-639, 1987.

Kennel, C., F. V. Coroniti, and F. L. Scarf, Plasma waves in magnetotail flux ropes, J. Geophys. Res., 91, 1424-1438, 1986.

Lester, M., W. J. Hughes, and H. J. Singer, Polarization patterns of Pi 2 magnetic pulsations and the substorm current wedge, J. Geophys. Res., 88, 7958-7966, 1983.

Maezawa, K., Magnetotail boundary motion associated with geomagnetic substorms, J. Geophys. Res., 80, 3543-3548, 1975.

Nagai, T., Field-aligned currents associated with substorms in the vicinity of synchronous orbit 2. GOES 2 and GOES 3 observations, J. Geophys. Res., 92, 2432-2446, 1987.

Richardson, I. G., and S. W. H. Cowley, Plasmoid-associated energetic ion bursts in the deep geomagnetic tail: properties of the boundary layer, J. Geophys. Res., 90, 12133-12158, 1985.

Richardson, I. G., S. W. H. Cowley, E. W. Hones, Jr., and S. J. Bame, Plasmoid-associated energetic ion bursts in the deep geomagnetic tail: properties of plasmoids and the postplasmoid plasma sheet, J. Geophys. Res., 92, 9997-10013, 1987.

Richardson, I. G., C. J. Owen, S. W. H. Cowley, A. B. Galvin, T. R. Sanderson, M. Scholer, J. A. Slavin, and R. D. Zwickl, ISEE-3 observations during the CDAW-8 intervals: Case studies of the distant geomagnetic tail covering a wide range of geomagnetic activity, This Issue, 1988.

Rostoker, G., S. -I. Akasofu, J. Foster, R. A. Greenwald, Y. Kamide, K. Kawasaki, A. T. Y. Lui, R. L. McPherron, and C. T. Russell, Magnetospheric substorms - definition and signatures, J. Geophys. Res., 85, 1663-1668, 1980.

Schindler, K., and J. Birn, Self-consistent theory of time-dependent convection in the earth's magnetotail, J. Geophys. Res., 87, 2263-2275, 1982.

Scholer, M., G. Gloeckler, B. Klecker, F. M. Ipavich, D. Hovestadt, and E. J. Smith, Fast moving plasma structures in the distant magnetotail, J. Geophys. Res., 89, 6717-6727, 1984a.

Scholer, M., G. Gloeckler, D. Hovestadt, B. Klecker, and F. M. Ipavich, Characteristics of Plasmoidlike Structures in the Distant Magnetotail, J. Geophys. Res., 89, 8872-8876, 1984b.

Scholer, M., B. Klecker, D. Hovestadt, G. Gloeckler, F. M. Ipavich, and A. B. Galvin, Energetic particle characteristics of magnetotail flux ropes, Geophys. Res. Lett., 12, 191-194, 1985.

Sibeck, D. G., G. L. Siscoe, J. A. Slavin, E. J. Smith, S. J. Bame, and F. L. Scarf, Magnetotail flux ropes, Geophys. Res. Lett., 11, 1090-1093, 1984.

Singer, H. J., W. J. Hughes, C. Gelpi, and B. G. Ledley, Magnetic disturbances in the vicinity of synchronous orbit and the substorm current wedge: A case study, J. Geophys. Res., 90, 9583-9589, 1985.

Slavin, J. A., B. T. Tsurutani, E. J. Smith, D. E. Jones, and D. G. Sibeck, Average configuration of the distant (<220 R_E) magnetotail: initial ISEE-3 magnetic field results, Geophys. Res. Lett., 10, 973-976, 1983.

Slavin, J. A., E. J. Smith, B. T. Tsurutani, D. G. Sibeck, H. J. Singer, D. N. Baker, J. T. Gosling, E. W. Hones Jr., and F. L. Scarf, Substorm associated traveling compression regions in the distant tail: ISEE-3 geotail observations, Geophys. Res. Lett., 11, 657-660, 1984.

Slavin, J. A., D. N. Baker, J. D. Craven, R. C. Elphic, D. H. Fairfield, L. A. Frank, A. B. Galvin, W. J. Hughes, R. H. Manka, D. G. Mitchel, I. G. Richardson, T. R. Sanderson, D. J. Sibeck, H. J. Singer, E. J. Smith, and R. D. Zwickl, ISEE 3 observations of plasmoid structure and dynamics: CDAW-8, J. Geophys. Res., 93, This issue, 1988.

Smith, E. J., J. A. Slavin, R. D. Zwickl, and S. J. Bame, Shocks and storm sudden commencements, in Solar Wind-Magnetosphere Coupling, edited by Y. Kamide and J. A. Slavin, Terra Scientific Publ. Co., Tokyo, 345-365, 1986.

Spreiter, J. R. and S. S. Stahara, Magnetohydrodynamic and gasdynamic theories for planetary bow waves, in Collisionless Shocks in the Heliosphere: Reviews of Current Research, B. T Tsurutani and R. G. Stone editors, AGU Monograph 35, Washington D. C., 85-107, 1985.

Stahara, S. S., D. Klenke, B. C. Trudinger, and J. R. Spreiter, Application of advanced computational procedures for modeling solar-wind interactions with venus - theory and computer code, NASA Contractor report 3267, NASA Scientific and Technical Publication, Washington D. C., 1980.

Tsurutani, B. T., I. G. Richardson, R. M. Thorne, W. Butler, E. J. Smith, S. W. H. Cowley, S. P. Gary, S.-I. Akasofu, and R. D. Zwickl, Observation of the right-hand resonant ion beam instability in the distant plasma sheet boundary layer, J. Geophys. Res., 90, 12159-12172, 1985.

Wolfe, J. H., The large-scale structure of the solar wind, in Solar Wind, edited by C. P. Sonett et al., NASA SP-308, U. S. Government Printing Office, Washington, 170-196, 1972.

APPENDIX A: SUBSTORM ACTIVITY ON MARCH 25, 1983

In this section ground magnetograms and geosynchronous magnetic field and energetic particle data will be used to determine the onset or intensification times of geomagnetic substorms occurring between 0500 and 1400 UT on March 25 1983.   Figure 10 displays the B_x and B_y components for the AFGL stations which covers an approximately 60° longitude range near 54 latitude. The station St Johns to the east supplements this chain. Figure 11 displays B_x and B_y components (or the equivalent H and D components as the case may be) from a series of auroral zone stations spanning the Alaska-Canadian sector. Figure 12 illustrates energetic electron and proton fluxes and magnetic field magnitude, B, and field latitude angle, θ, from 5 different geosynchronous spacecraft.

The mid-latitude magnetograms of Figure 3 reveal the rapid development of a modest magnetic storm main phase after the ssc of 0544 UT. The decreasing magnitude of the B_x component is particularly evident at Guam due to the low latitude of this station and its location in the dusk quadrant where such decreases are particularly pronounced. This main phase begins developing without any clear substorm onset although ongoing magnetic activity at auroral latitudes is indicated by the Leirvogur magnetogram (not shown).

The first substorm intensification following the sudden commencement occurred at 0623 UT. Indicators are the onset of Pi2 pulsations at the sub auroral AFGL magnetometer chain (not shown), the onset of B_y perturbations at the same stations (Figure 10b), and similar B_y perturbations at the US observatories (Figure 3). The B_y perturbation changed sign between the AFGL stations Rapid City and Mount Clemens with the station in between, Camp Douglas, showing a positive-to-negative D change delayed about 4 minutes from
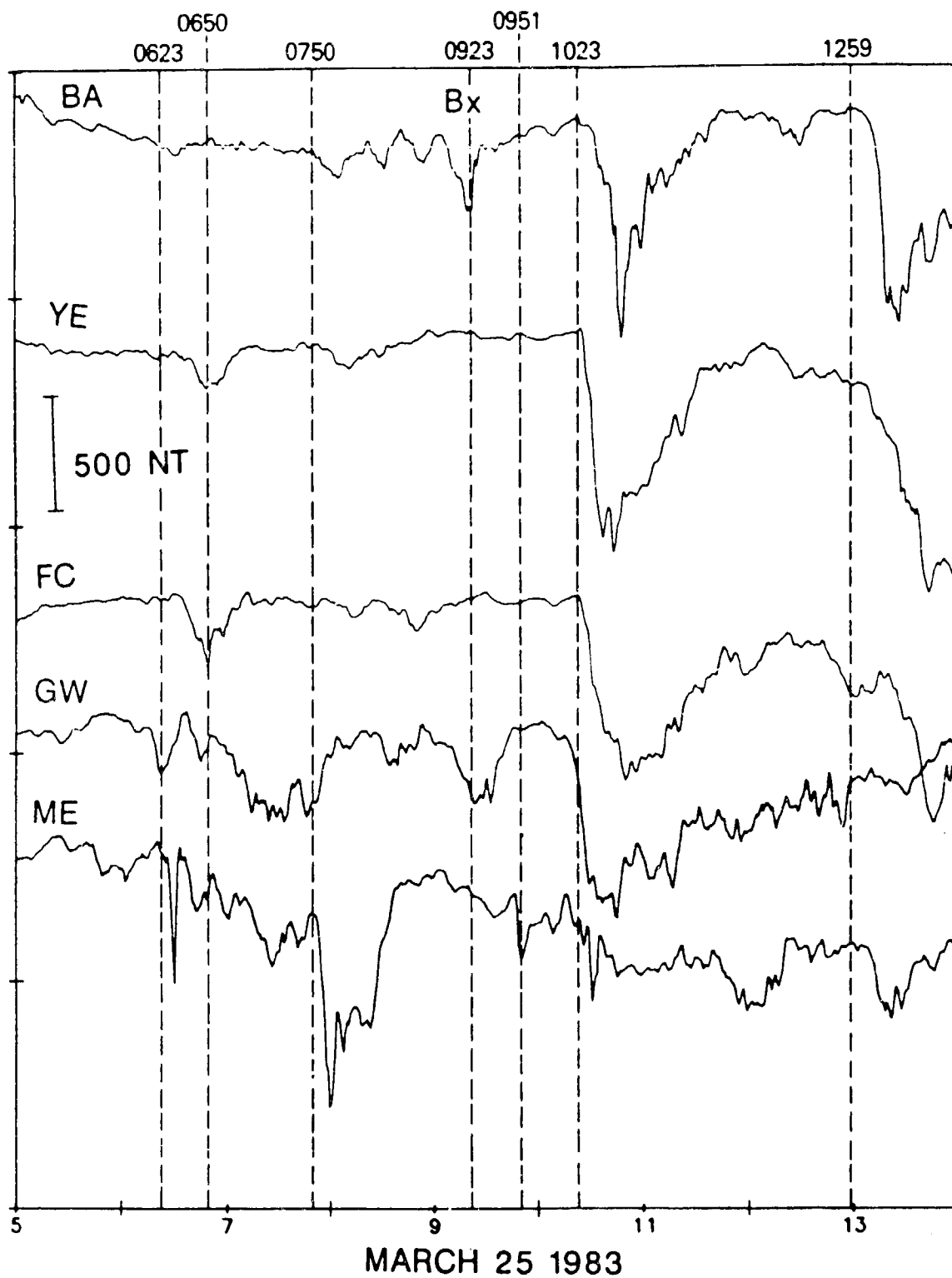
65

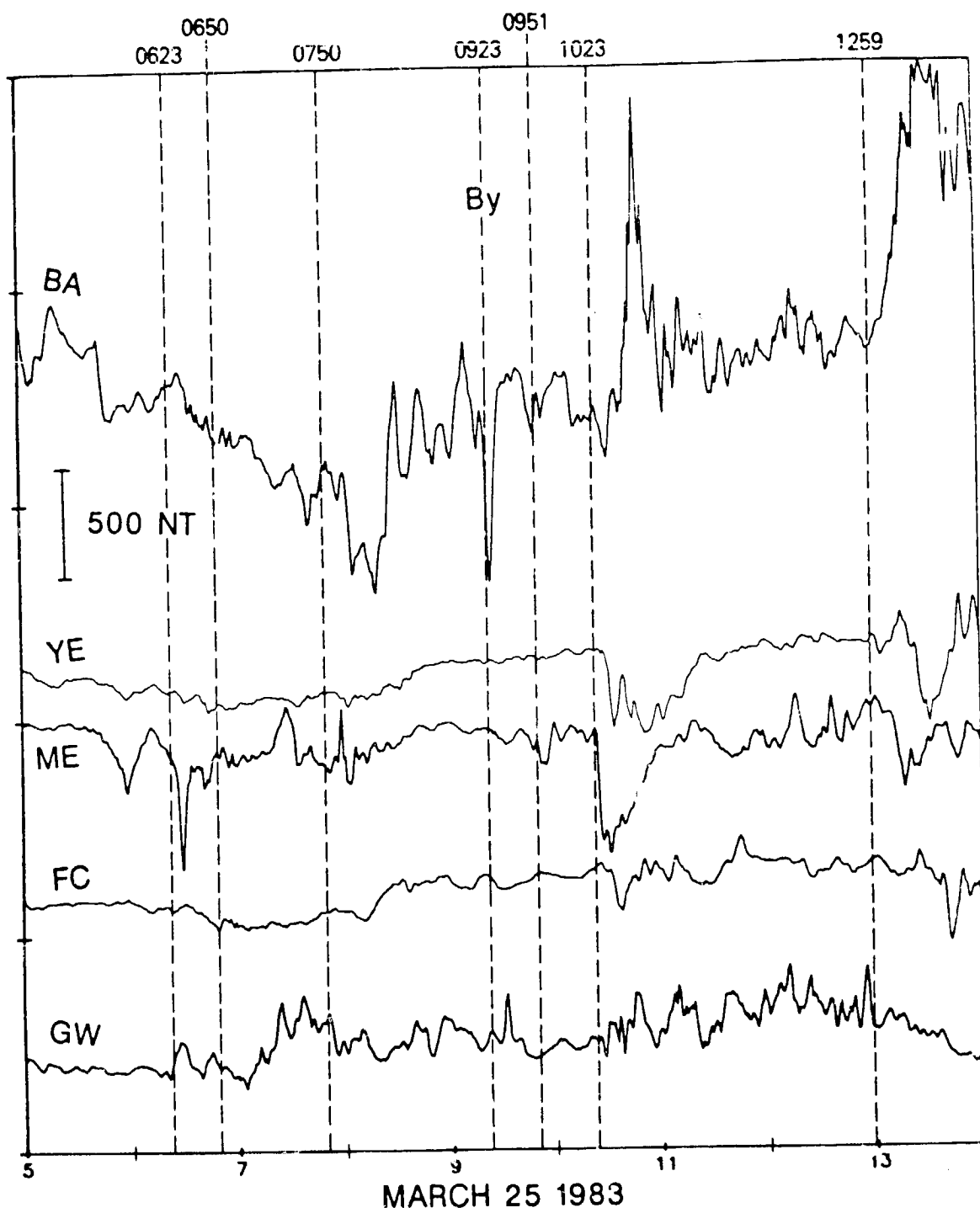Fig. 11a. B_x component magnetograms from auroral zone stations.

66

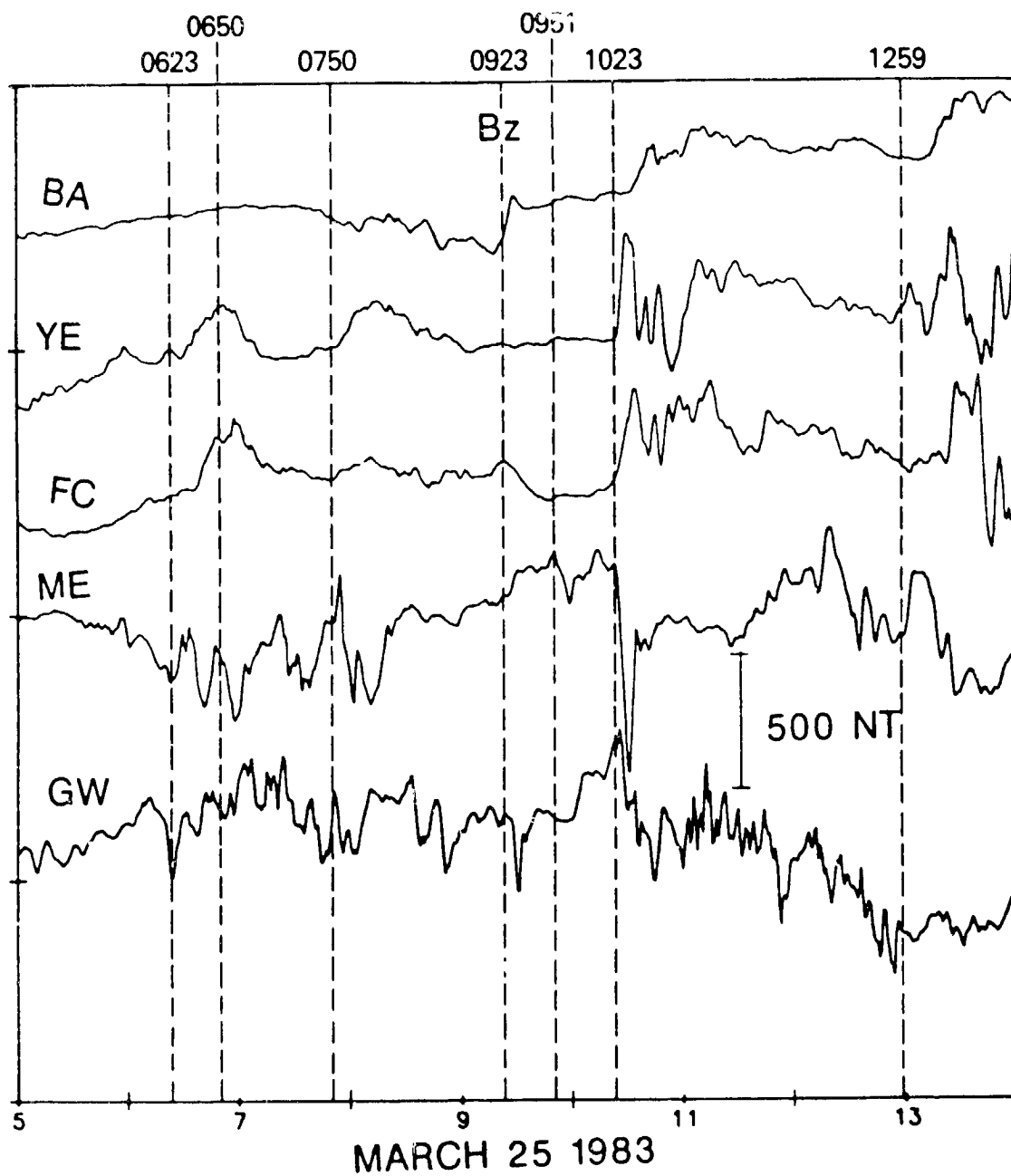Fig. 11b. Same as figure 11a for the B_y magnetogram components.

Fig. 11c. Same as figure 11c for the B_z magnetogram components.
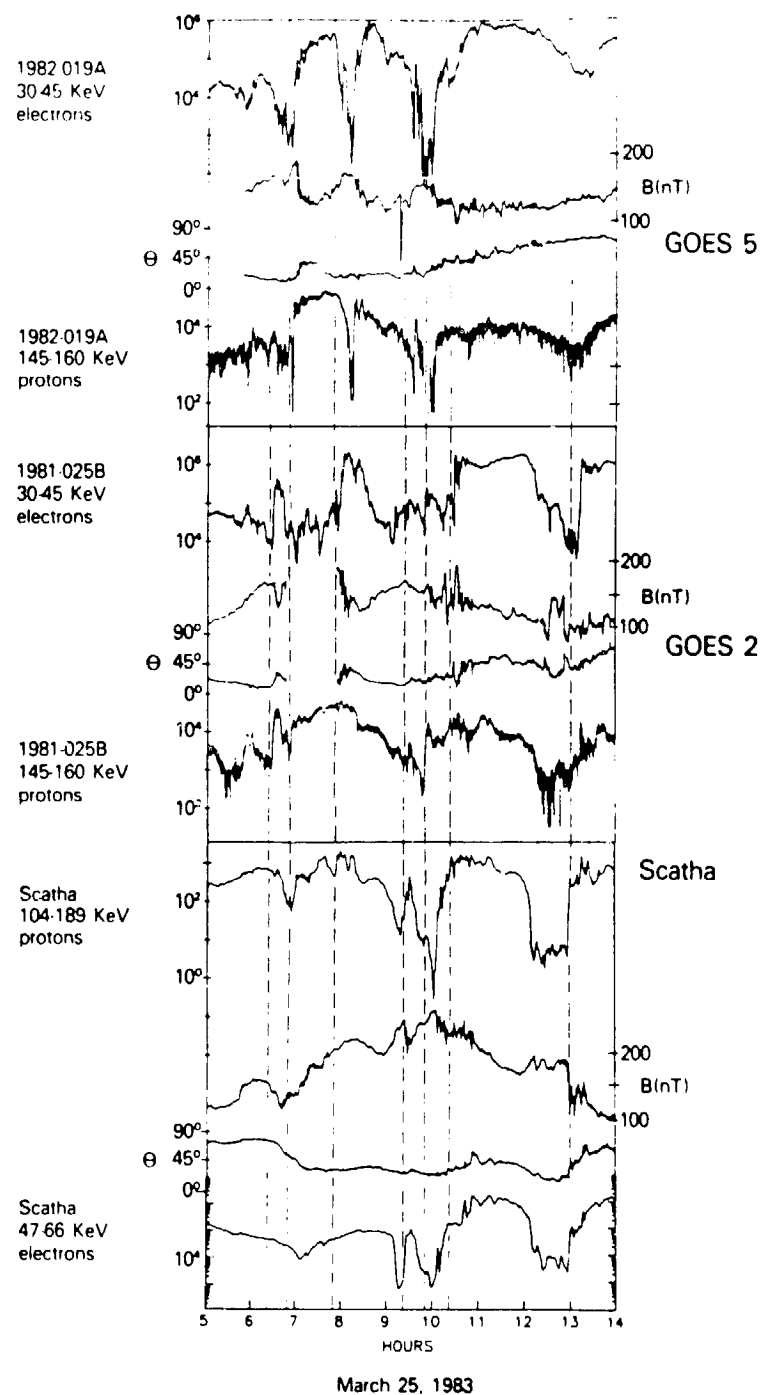
68

Fig. 12. Energetic electron and proton intensities and magnetic field magnitude and latitude angle from 5 different synchronous orbit spacecraft. Vertical dashed lines indicate substorm onset times deduced from these data and ground magnetograms.

the onset. This behavior locates the central meridian of the current wedge at Camp Douglas near 320° geomagnetic longitude or very near local midnight. This is consistent with both the data from GOES 2 near the same meridian (Figure 12) which showed an increase in the θ angle at 0624 and the data from 1981-025B which detected electron and proton increases three minutes later. GOES 5 and spacecraft 1982-019A at 1:30 LT saw no effects. Stations to the west of the onset (Glenlea (not shown), Rapid City (Figure 10), Tucson, Boulder, and Lompoc (Figure 3)) exhibited a reversal of this initially positive B_y perturbation over the following 30 minutes which is indicative of a westward movement of the wedge. The latitude of the auroral electrojet associated with this current wedge was north of Glenlea (59.5° but well south of Churchill (68.8°) and Lynn Lake (67.3°) since no significant effects were seen at the latter location. The wedge was confined to no more than 2 or 3 hours of local time.

At 0650 a further substorm intensification was indicated by positive B_y at Sudbury (Figure 10), and Fredricksburg (not shown) with similar, slightly delayed perturbations at Mt Clemens, Camp Douglas, and Rapid City. Further to the east San Juan saw no significant D perturbation but experienced a positive H perturbation at 0654 (not shown). Pi2 pulsations at the AFGL chain tend to confirm the 0650 onset time although ongoing pulsation activity tend to obscure the new intensification. Evidence for the auroral electrojet associated with these perturbations comes from a negative perturbation at Great Whale River and even St Johns (Figure 10) beginning near 0650. The wedge apparently was centered near 10° longitude or at least 2 hours past local midnight. This interpretation is consistent with an observed dipolarization at GOES 5 that began slowly near 0650 UT when this spacecraft was near the local time of the onset and an increase in energetic electrons and ions at 1982-019A at 0655 UT

at a location only 7° west of GOES 5. This event had little effect on particles measured by 1981-025B in the region just before midnight. The data are missing at GOES 2.

Pi2 pulsations and magnetogram component changes indicated that the next important intensification occurred at 0750 UT. Positive B_y perturbations occurred at Newport (Figure 10) and Lompoc (Figure 3), and negative B_y perturbations occurred at Rapid City, Camp Douglas, Mt Clemens (Figure 10) and Boulder (Figure 3). Positive H bays were seen at Rapid City, Newport, (Figure 10) Tucson and Boulder and slightly later at Lompoc (Figure 3). The auroral electrojet was apparently near Meanook judging from a large sharp negative B_x perturbation at 0750 that was accompanied by little B_z perturbation. These observations place the onset near 310° longitude or very near local midnight. A field dipolarization was detected by GOES 2 at 0753 UT near 0100 LT but not at GOES 5 near 0300 LT. At 2300 LT, intense fluxes of energetic electrons at 1981-025B increased even more at 0759 UT and the field angle computed from the electron anisotropy (not shown) [Baker et al., 1981] also increased. At 0300 LT spacecraft 1982-019A detected a brief electron increase at 0800 UT that was superimposed on a decreasing trend. Further variations of magnetograms in the subsequent half hour suggest the possibility of further intensifications, but it is difficult to distinguish spatial motion of current systems from time changes in intensity during this complicated interval.

A rather minor intensification occurred at a time which is tentatively placed at 0923 UT. The event was apparently centered near 0100 LT as deduced from positive B_y at Victoria (not shown) and Newport and negative B_y's at Rapid City and stations to the east along with positive H bays at Boulder, Tucson, Lompoc, Rapid City and Newport. Little evidence was seen for the auroral

electrojet although there was a large negative B_y perturbation at Barrow. GOES 2 (0230 LT) saw a small dipolarization beginning at 0923 and spacecraft 1981-025B saw a small increase in energetic protons at 0928 UT. Scatha at 1930 LT saw a particle increase and a small dipolarization but this may be unrelated to the event near midnight at such an early local time.

Another intensification was marked by positive B_y perturbations at Mt Clemens, Camp Douglas at 0951 and at Rapid City, Boulder and Tucson further to the west a few minutes later. Negative By occurred at San Juan (not shown) and Sudbury; these negative perturbations were more gradual but occurred at an earlier time of about 0946. Positive bays occurred at Fredricksburg and San Juan (not shown) and Sudbury at 0951. This event therefore appeared to be centered near 350° which places it at the unusual location of 0400 LT. These ground observations are supported by the satellite data. GOES 5 near 0500 LT detected a theta increase at 0946 UT but GOES 2 near 0300 observed only a small increase near this time. Spacecraft 1981-025B near the 0100 LT observed electron and ion increases at 0949 UT. Spacecraft 1982-019A detected a large increase in electrons and ions but not until 0959 UT (0500 LT).

A very significant intensification occurred at 1023 UT. Most midlatitude stations within North America detected negative By perturbations with the stations more to the west exhibiting the reversal from the earlier positive perturbation at a somewhat later time. The likely local time of the current wedge center would appear to be near the west coast of North America or near 0200 LT. This event in contrast to the intensifications during the previous 2 hours, produced very large negative bays at the stations above 64° geomagnetic latitude. Onset times were College 1027 UT, Yellowknife 1025 UT Churchill 1024 UT. There was a small dipolarization at Scatha (2130 LT) at 1019 UT. GOES 2

near 0300 LT detected high levels of fluctuations but no clear dipolarization and GOES 5 had moved too far to the east to see any effects. The 1981-025B energetic electrons intensity increased at 1027 UT (0130 LT) and the inferred field angle computed from the electron distributions showed a large increase at the same time. Energetic electrons at spacecraft 1982-019A also showed an increase at 1030 UT even though this spacecraft had almost reached the dawn meridian.

By 1200 UT the SCATHA spacecraft was approaching the midnight meridian. SCATHA saw a classical stretching of the field [Baker et al., 1981] and disappearance of energetic particles followed by an abrupt dipolarization and particle return at 1259. This large onset produced negative, midlatitude B_y's throughout the North American sector and as far west as Honolulu (not shown). A large positive H at Guam with no B_j perturbation marked this longitude (2200 LT) as near the onset meridian. Large negative H bays are seen at College and Canaa.an observatories to the east. The other synchronous orbit spacecraft had moved well to the east by this time and saw only delayed particle increases.

In conclusion, we have identified seven times of significant substorm onsets or intensifications as are marked on the figures. It should be appreciated, however that during this complex interval of ongoing activity there are probably other times of increases in field aligned current systems with lesser magnitudes and smaller spatial scales that can effect individual observing points both on the ground and in space. We feel that the seven events are the most reasonable choices for comparisons with data in the deeper magnetotail.

LABORATORY OPERATIONS

The Aerospace Corporation functions as an "architect-engineer" for national security projects, specializing in advanced military space systems. Providing research support, the corporation's Laboratory Operations conducts experimental and theoretical investigations that focus on the application of scientific and technical advances to such systems. Vital to the success of these investigations is the technical staff's wide-ranging expertise and its ability to stay current with new developments. This expertise is enhanced by a research program aimed at dealing with the many problems associated with rapidly evolving space systems. Contributing their capabilities to the research effort are these individual laboratories:

Aerophysics Laboratory: Launch vehicle and reentry fluid mechanics, heat transfer and flight dynamics; chemical and electric propulsion, propellant chemistry, chemical dynamics, environmental chemistry, trace detection; spacecraft structural mechanics, contamination, thermal and structural control; high temperature thermomechanics, gas kinetics and radiation; cw and pulsed chemical and excimer laser development including chemical kinetics, spectroscopy, optical resonators, beam control, atmospheric propagation, laser effects and countermeasures.

Chemistry and Physics Laboratory: Atmospheric chemical reactions, atmospheric optics, light scattering, state-specific chemical reactions and radiative signatures of missile plumes, sensor out-of-field-of-view rejection, applied laser spectroscopy, laser chemistry, laser optoelectronics, solar cell physics, battery electrochemistry, space vacuum and radiation effects on materials, lubrication and surface phenomena, thermionic emission, photo-sensitive materials and detectors, atomic frequency standards, and environmental chemistry.

Computer Science Laboratory: Program verification, program translation, performance-sensitive system design, distributed architectures for spaceborne computers, fault-tolerant computer systems, artificial intelligence, micro-electronics applications, communication protocols, and computer security.

Electronics Research Laboratory: Microelectronics, solid-state device physics, compound semiconductors, radiation hardening; electro-optics, quantum electronics, solid-state lasers, optical propagation and communications; microwave semiconductor devices, microwave/millimeter wave measurements, diagnostics and radiometry, microwave/millimeter wave thermionic devices; atomic time and frequency standards; antennas, rf systems, electromagnetic propagation phenomena, space communication systems.

Materials Sciences Laboratory: Development of new materials: metals, alloys, ceramics, polymers and their composites, and new forms of carbon; non-destructive evaluation, component failure analysis and reliability; fracture mechanics and stress corrosion; analysis and evaluation of materials at cryogenic and elevated temperatures as well as in space and energy-induced environments.

Space Sciences Laboratory: Magnetospheric, auroral and cosmic ray physics, wave-particle interactions, magnetospheric plasma waves; atmospheric and ionospheric physics, density and composition of the upper atmosphere, remote sensing using atmospheric radiation; solar physics, infrared astronomy, infrared signature analysis; effects of solar activity, magnetic storms and nuclear explosions on the earth's atmosphere, ionosphere and magnetosphere; effects of electromagnetic and particulate radiations on space systems; space instrumentation.

...